Role of ZBTB18 Tumor Suppression in Glioblastoma Progression

Authors: Marzieh Hesam Mohammadi

Submitted: 5. September 2024
Published: 4. November 2024
Volume: 11
Issue: 6

Affiliation: Faculty of Pharmacy and Biochemistry, University of Buenos Aires, Argentina and Faculty of Medicine, University of Freiburg, Germany

Languages: English
Keywords: Glioblastoma, ZBTB18, SREBP Pathway, Tumor Suppressor, CRISPR/Cas9 Knockdown
Categories: Medicine, Demetrios Project
DOI: 10.17160/josha.11.6.1011

Abstract:

Glioblastoma (GBM) is the most frequent and most malignant human brain tumor which consists of distinct subtypes characterized by their gene expression profile. The Zinc Finger and BTB Domain Containing 18 (ZBTB18) is a transcriptional repressor that plays a crucial role in brain development and neuronal differentiation. A previous study in Carro 's group provided evidence of the role of ZBTB18 in a network of transcription factors that control mesenchymal transformation in GBM. More recently, our group displayed that ZBTB18 overexpression leads to a loss of the mesenchymal and proliferative signatures and downregulation of an array of genes involved in glioblastoma tumorigenesis. These surveys support the role of ZBTB18 as a tumor suppressor in GBM and raise further questions as to how this is carried out in different tumor samples. Our project "Role of ZBTB18 tumor suppressor in Glioblastoma progression" pointed out to describe some of the mechanisms by which ZBTB18 targets lead to glioblastoma

the effect of Corin inhibition of HDAC and LSD1 which has been shown to act as a dual inhibitor. qPCR analysis revealed that Corin negatively regulates SREBP genes and affects the rate of ATP production. Given the lack of effective therapies for GBM, more studies on the linkage between the role of ZBTB18 and fatty acids synthesis in tumorigenesis could have future therapeutical applications.

Role of ZBTB18 tumor suppressor in Glioblastoma progression

For the degree of Master of Science

Author: Marzieh Hesam Mohammadi

Cohort: 2020-2022

Director: PD Dr. Maria Stella Carro

Co- Director: Prof. Dr. Stella Maris Ranuncolo

Faculty of Pharmacy and Biochemistry, Faculty of Medicine –
Universidad de Buenos Aires, Argentina

Faculty of Medicine –
Albert Ludwigs University of Freiburg, Germany

2022

Author: Marzieh Hesam Mohammadi

Director: PD Dr. Maria Stella Carro

Co- Director: Prof. Dr. Stella Maris Ranuncolo

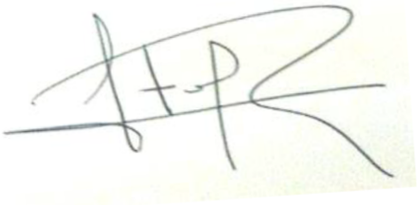

Master of Science in Biomedical Sciences

Statement for the Master's Thesis

Hereby I confirm that

- I completed the submitted master's thesis independently.
- I used no sources or aids other than those stated and all verbatim or conceptual content taken from other works has been identified as such.
- the submitted master's thesis was or is not, either in full or in large part the subject of another examination process.
- the electronic version of the master's thesis submitted is in content and format the same as the printed version, and
- the master's thesis has not yet been published.

15.01.2022	**Marzieh Hesam Mohammadi**	
Date	Name, Firstname	Signature

Hereby I declare on oath that I wrote my Master Thesis myself and did not use other sources than mentioned as resources.

15.01.2022	**Hesam Mohammadi, Marzieh**	
Date	Name, First Name	Signature of the student

The Master Thesis can be accessible to the public 24 months after the completion of the procedure.

15.01.2022
Date

Signature of the student
Name: Marzieh Hesam Mohammadi

15.01.2022
Date

Signature of the Director
Name: PD Dr. Maria Stella Carro

15.01.2022
Date

Signature of the Co-Director
Name: Prof. Dr. Stella Maris Ranuncolo

Table of Contents

Abstract

Glioblastoma (GBM) is the most frequent and most malignant human brain tumor which consists of distinct subtypes characterized by their gene expression profile. The Zinc Finger and BTB Domain Containing 18 (ZBTB18) is a transcriptional repressor that plays a crucial role in brain development and neuronal differentiation. A previous study in Carro 's group provided evidence of the role of ZBTB18 in a network of transcription factors that control mesenchymal transformation in GBM. More recently, our group displayed that ZBTB18 overexpression leads to a loss of the mesenchymal and proliferative signatures and downregulation of an array of genes involved in glioblastoma tumorigenesis. These surveys support the role of ZBTB18 as a tumor suppressor in GBM and raise further questions as to how this is carried out in different tumor samples. Our project "Role of ZBTB18 tumor suppressor in Glioblastoma progression" pointed out to describe some of the mechanisms by which ZBTB18 targets lead to glioblastoma progression. Recently, Dr. Carro's group has reported that ZBTB18 regulates the expression of SREBP genes, which are involved in the fatty acid synthesis. Here, this study aims at better defining the significance of SREBP pathway activation in glioblastoma and its potential involvement in the previously observed ZBTB18 tumor suppressive function. To achieve this goal, we attempted to treat various Brain Tumor Stem-like Cells (BTSC) (BTSC168 and BTSC233 cells) with oxLDL which has been reported to activate the SREBP pathway. To determine the correct conditions for oxLDL treatment, we first set up a time-course experiment and analyzed the expression of several SREBP genes by qPCR. This experiment due to technical reasons that still need to be clarified, did not allow us to rule out whether ZBTB18-mediated downregulation of SREBP genes is important for ZBTB18 tumor suppressor activity. We then planned to analyze in more detail the ZBTB18 function by performing CRISPR/Cas9 knockdown in the BTSC475 cells which express ZBTB18. Interestingly, ZBTB18 knockdown positively regulated a subset of SREBP genes. In line with our findings, we observed an increase of lipid droplets upon ZBTB18 knockdown; the overall metabolism, however, was not particularly affected. Finally, as LSD1 and HDAC are implicated in SREBP activation, we investigated the effect of Corin inhibition of HDAC and LSC1 which has been shown to act as a dual inhibitor. qPCR analysis revealed that Corin negatively regulates SREBP genes and affects the rate of ATP production. Given the lack of effective therapies for GBM, more studies on the linkage between the role of ZBTB18 and fatty acids synthesis in tumorigenesis could have future therapeutical applications.

Acknowledgments

I would like to thank the following people who have helped me to write and complete this thesis:

First and foremost, my director PD Dr. Maria Stella Carro for her unstinting support, perceptiveness, and patience; This project would not have been done without her guidance and feedback. I have to thank her for her criticisms, reliability, and always being reachable even in off-hours.

Prof. em. Dr. Drs. h.c. Roland Mertelsmann dean of the IMBS program, the director of the program Prof. Dr. Dres. h.c. Christoph Borner, and the coordinator Bärbel Schätzle, for their generous financial backing, endless, and continuous advice and encouragement, and being deeply sympathetic in dire straits; Without their special attention, I would not be here today and I will never ever forget them.

Prof. Dr. Cristina Arranz and Prof. Dr. Marta Mollerach at the University of Buenos Aires, Argentina for their tremendous support during the uncertain situation of the pandemic.

Prof. Dr. Stella Maris Ranuncolo for her kind supervision as a co-director from UBA.

My lab colleagues for the friendly atmosphere that they created, especially Dr. Roberto Ferrarese for his valuable and detailed advice, and also Eva Kling and Verena Hasse for their enormous help.

The University of Freiburg for awarding a DAHZ/CUAA scholarship.

I also should not forget to thank my family, especially my parents for their unconditional support, uninterrupted reliance, devotion, and affection. I am also indebted to my uncle who was always backing and encouraging me. Also, I am grateful to my Iranian friends who did not leave me alone, supported me with whatever they could, and enheartened me whenever I was disheartened.

Abbreviations

ATP	Adenosine triphosphate
APS	Ammonium peroxodisulfate
BTSCs	Brain Tumor Stem-like Cells
BBB	Blood-brain barrier
CDK6	Cyclin-dependent kinase 6
CDKN2A	CDK inhibitor N2A
CTBP	C-terminal binding proteins
CNS	Central nervous system
co-IP	Coimmunoprecipitation
cDNA	Converse Deoxyribonucleic acid
DMEM	Dulbecco's Modified Eagle's Medium
ERR	Excess relative risk
EGFR	Epidermal growth factor receptor
ECAR	Extracellular acidification rate
EV	Empty vector
FDA	Food and Drug Administration
FASN	Fatty acid synthase
GBM	Glioblastoma multiforme
GPAM	Glycerol-3-phosphate acyltransferase
GNPs	Mouse gliomas
HRP	Horse reddish peroxidase
HATs	Histone acetyltransferases
HDAC	Histone Deacetylase
HGG	High-grade gliomas
IDH	Isocitrate dehydrogenase
LDLR	Low density lipoprotein receptor
LSS	Lanosterol synthase
LSD1	Lysine-specific demethylase 1
LDs	Lipid droplets
MS	Mass spectrometry
mRNA	Messenger RNA
MES	Mesenchymal
MGES	Mesenchymal gene expression signature
MGMT	O6-methylguanine methyltransferase

NSCs	Neural stem cells
OPCs	Oligodendrocyte precursor cells
oxLDL	Low-Density Lipoprotein from Human Plasma, oxidized
OCR	Oxygen consumption rate
PN	Proneural
PDGFRα	Platelet-derived growth factor receptor α
PCR	Polymerase Chain Reaction
PTEN	Phosphatase and tensin homolog
PBS	Phosphate-buffered saline
q-RT-PCR	Quantitative Real-Time PCR
RNA	Ribonucleic acid
RIPA	Radioimmunoprecipitation assay
STAT3	Signal transducer and activator of transcription 3
SQLE	Squalene epoxidase
SCD	Stearoyl-CoA desaturase
SREBPs	Sterol regulatory element-binding proteins
SDS	Sodium dodecyl sulfate
SOAT1	Sterol-O transferase
SDS-PAGE	Sodium dodecyl sulfate-polyacrylamide gel electrophoresis
sgRNAs	small guide RNAs
TAE	Tris Acetate EDTA
TCGA	The Cancer Genome Atlas
TFs	Transcription factors
TEMED	Tetramethylethylene diamine
WHO	Word Health Organization
ZBTB18	Zing Finger and BTB Domain Containing 18
ZBTB18_mut	ZBTB18 mutant

1 Introduction

1.1 Glioblastoma multiforme

Glioblastoma multiforme (GBM) is an aggressive type of cancer (WHO grade IV glioma), arising from glia cells or their precursors in the central nervous system (CNS). It is known as the most malignant primary brain tumor with a 5-year survival of 7.2%, characterized by a highly invasive nature, poor prognosis, and resistance to conventional therapies (Holland EC, 2000; Fedele et al., 2017). Glioblastoma is also the most frequent primary CNS cancer with a 4.5-11.2 incidence and 1.6-8.5 cases per 100,000 men and women respectively during adulthood in Europe and increases with age in the United States (Crocetti et al., 2012; Wei Wu et al., 2021).

Several studies have shown that GBM originates from neural stem cells (NSCs), oligodendrocyte precursor cells (OPCs), and NSC-derived astrocytes and causes different behaviors in animal models due to various cellular origins (Zhu et.al, 2005; Chow et.al, 2011; Liu et.al, 2011; Wu W et.al, 2021) (Fig. 1).

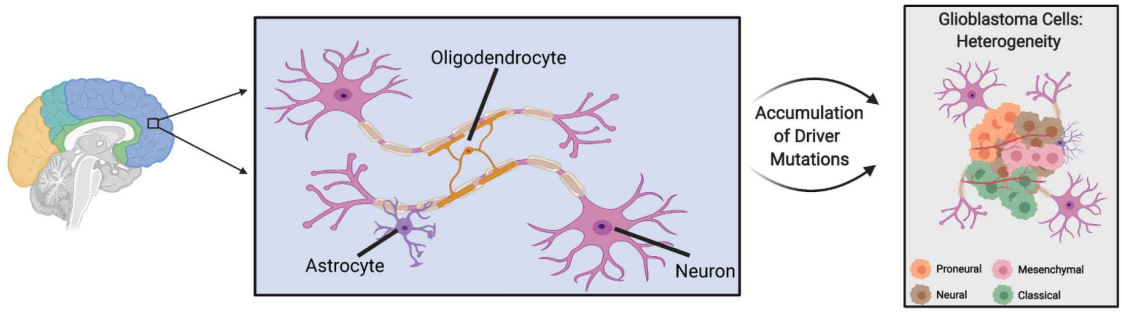

Figure 1: Glioblastoma multiform (GBM) heterogeneity (right box) regarding cell of origin (left box). GBM drives from three types of brain parenchyma cells: neural stem cells (NSCs), NSC-derived astrocytes, and oligodendrocyte precursor cells (OPCs). GBM are characterized by a strong heterogeneity (intertumor and intratumor), in particular, GBM can be classified in four sub-groups (mesenchymal, classical, proneural, and neural), which can co-exist in the same tumor (Wu W et.al, 2021).

The etiology of GBM is still uncharted; however, some risk factors such as ionizing radiation exposure have been related to an increased risk of GBM development (Wu W et.al, 2021). The symptoms depend on the localization of the GBM and most common are headache, weakness, memory loss/confusion, seizure, speech changes, visual changes, and loss of consciousness (Mrowczynski et al., 2021).

The standard treatment for GBMs is complex; it is initially comprised of maximal surgical resection that depends on the localization of the tumor and the size followed by chemoradiotherapy using temozolomide (TMZ) (Wu W et.al, 2021; Tamimi and Juweid, 2017). However, incomplete resection, exclusive blood-brain barrier (BBB), high degree of genetic heterogeneity, and immunosuppressive microenvironment are still enumerated as the most ongoing challenges for the GBM treatment. Besides, resistance against all current treatment modalities is promoted by robust DNA repair and self-renewing capability in glioblastoma cells (Wu W et.al, 2021).

1.2 Glioma's classification

According to the World Health Organization (WHO) criteria, four groups of gliomas have been defined. This assessment is comprised of the morphology of CNS tumors, grade of malignancy (grade I–IV), proliferative index, their response to treatment, and patients' survival. Grade I, II, and III contain non-malignant, relatively non-malignant, and low-grade malignancy tumors respectively while grade IV designates the highest biological behavior tumors known as Glioblastoma Multiforme (GBM) (Urbańska et al., 2014; Kleihues et al., 1995).

Differential diagnosis between primary and secondary glioblastoma is clinically and biologically important. A short clinical history shows the primary (de novo) glioblastomas have a rapid clinical presentation without evidence of less malignant precursor lesions while secondary glioblastomas grow more slowly, and progress from low-grade (WHO grade II) or anaplastic astrocytoma (WHO grade III) (Ohgaki et al., 2004).

1.3 Glioma molecular subclasses

The molecular profile of low-grade gliomas and secondary GBMs is important as they are considerably different at the genetic and epigenetic levels (Goodenberger et al., 2012).

Primary GBM typically observed in older patients (commonly without prior clinical evidence) mostly shows *EGFR* amplification/overexpression, *PTEN* mutations, *p16* deletions while secondary GBM with a various clinical history occurs in younger patients often presents *TP53* mutations even in the earliest detectable alteration (Kleihues et al., 2000; Maher et al., 2001).

Among all genetic and epigenetic alterations in GBM, three important molecular markers have been reported predictive or prognostic from clinical implications point of view: *1p/19q* codeletion (lack of chromosomal arms 1p and 19q), *IDH1/IDH2* (isocitrate dehydrogenase) mutations, and O^6-methylguanine methyltransferase (*MGMT*) promoter methylation (Riemenschneider et al., 2010; Tabatabai et al., 2010).

IDH1 has a crucial rule is the citric acid (Krebs) cycle and its function as an enzyme is to generate adenosine triphosphate (ATP) for cellular energy. *IDH1* recurrent mutations observed in 12% of GBM patients mostly in secondary GBMs related to survival enhancement (Parsons et al., 2008; Agnihotri et al., 2014).

MGMT promoter methylation commonly happened at the earliest level of GBM development and potentially characterized only as a predictive marker for alkylating agent chemotherapy. Known *MGMT* function is to repair O^6-methylguanine that is a very toxic and mutagenic DNA adducts (Tabatabai et al., 2010; Mulholland et al., 2012).

In 2006, Phillips and colleagues, identified a frequent pattern of disease progression into the mesenchymal phenotype which was suggesting that the molecular classification of glioblastoma could be important to predict a targeted therapy's response (Phillips et al., 2006). In particular, the mesenchymal subgroup was identified as the most aggressive one associated with the worst clinical outcome.

According to the latest molecular classification based on gene expression (Verhaak et al., 2010), GBMs are divided into classical, mesenchymal (MES), proneural (PN), and neural subtypes. Further studies revealed that various subtypes of GBM respond differently to

treatment and they showed that each of them was enriched for different mutations and genomic alterations (Verhaak et al., 2010; Agnihotri et al., 2014).

In particular, the proneural subgroup was enhanced for *IDH1/2* and *TP53* mutations, *PDGFR*a amplifications, *CDK4*, cyclin-dependent kinase 6 (*CDK6*), and *MET*. *IDH1* mutations also was enriched in high percentage of young adults. The classical subtype is recognized by loss of phosphatase and tensin homolog (*PTEN*) and *EGFR* amplification. The mesenchymal subclass is related to low overall survival, consist of neurofibromatosis Type 1 mutations, loss of *TP53* and CDK inhibitor N2A (*CDKN2A*). The neural subtype also is enriched neuronal marker like *NEFL* without more specific feature compared to other classes. The others; oligodendroglioma, oligoastrocytoma, and diffuse astrocytoma, all has a same PN gene signature (62) which act like *IDH1* mutations. GBM molecular subtypes with unique methylation pattern and gene expression profiles are depicted in Figure 2. This supports that each subtype arises from a different cell of origin (Agnihotri et al., 2014).

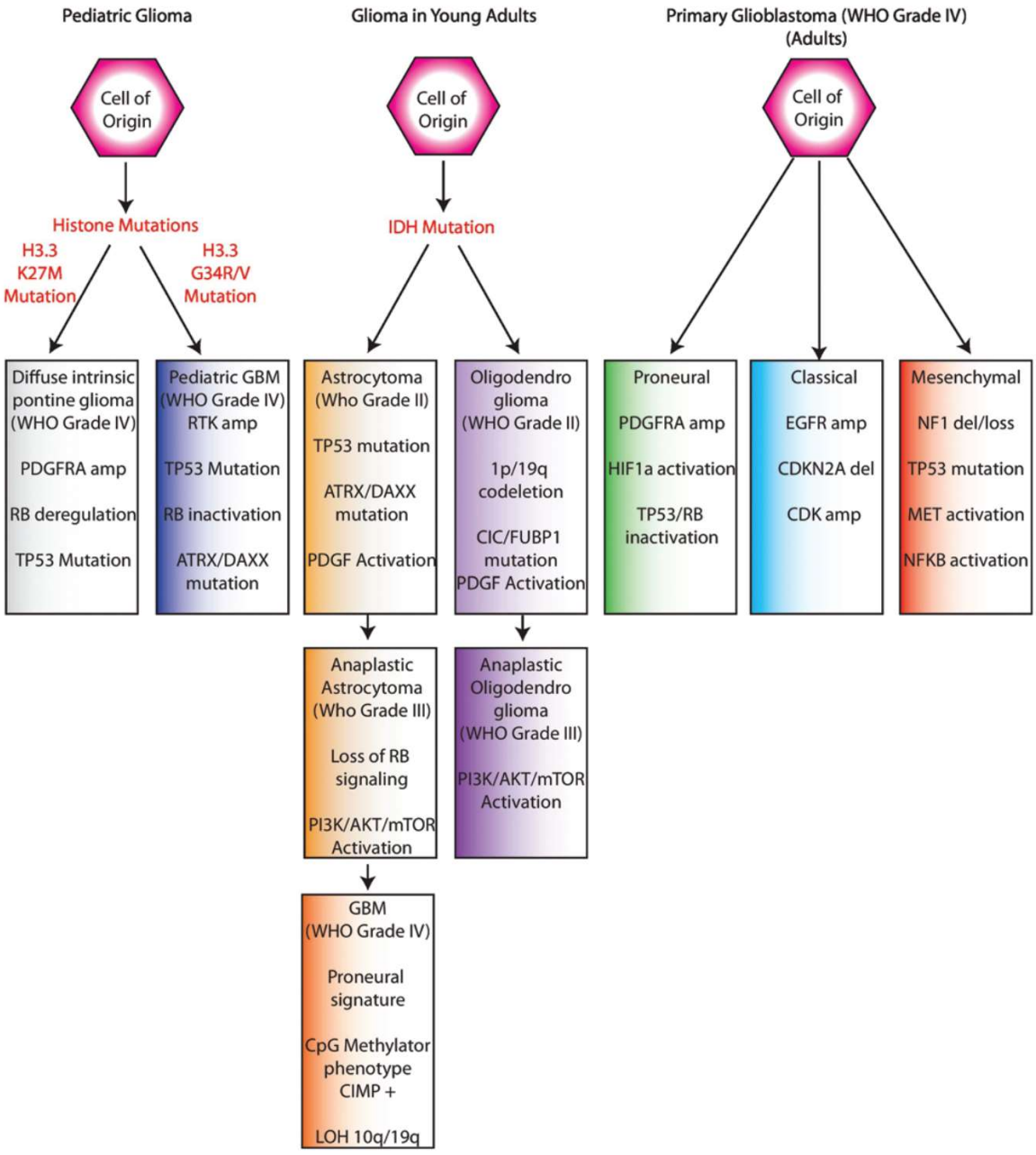

Figure 2: Transcriptional networks of pediatric and adult gliomas according to the molecular and genetic changes. amp = amplification; del = deletion; MET = multiple receptor tyrosine; PDGFRA = PDGFRa; RB = retinoblastoma; RTK = receptor tyrosine kinase (Agnihotri et al., 2014).

The glioma subtypes show different genetic pathways alterations and affect patients with different ages. Some factors contribute to the evolution of glioblastomas such as oncogenes (*EGFR*, *PDGF* and its receptors) and tumor suppressor genes (*p16INK4a*, *p14ARF*, *PTEN*, *RB1*, and *TP53*) (Ohgaki et al., 2004). Some processes regulating cell fate choices lead to glioma aggressiveness during neurogenesis. Table 1 depicts the phenotype of tumor subtypes from WHO stages, in relation the gene expression subtype, is explained (Phillips et al., 2006).

	Proneural	**Proliferative**	**Mesenchymal**
Histological grade	WHO grade III or WHO grade IV with or without necrosis	WHO grade IV with necrosis	WHO grade IV with necrosis
Cellular morphology	Astrocytic or Oligodendroglial	Astrocytic	Astrocytic
Evolution of signature	Arises in 1° tumor, may persist or convert to *Mes*	Arises in 1° tumor, may persist or convert to *Mes*	Arises in 1° tumor or by conversion from other subtype
Patient age	Younger (~40 yrs.)	Older (~50 yrs.)	Older (~50 yrs.)
Prognosis	Longer survival	Short survival	Short survival
Histological Markers	Olig2, DLL3, BCAN	PCNA, TOP2A	CHI3L1/YKL40, CD44, VEGF
Tissue similarities	Adult and Fetal Brain	HSC, lymphoblast	Bone, cartilage, smooth musc, endothelium, dendritic cells
Biological process	Neurogenesis	Proliferation	Angiogenesis
Analogous forebrain cell	Neuroblast	Neural Stem Cell and/or Transit Amplifying Cell	Neural Stem Cell
Chromosome gain/loss	None	Gain of 7 & Loss of 10 or 10q	Gain of 7 & Loss of 10
PTEN locus	PTEN intact	PTEN loss	PTEN loss
EGFR locus	EGFR normal	EGFR amplified or normal	EGFR amplified or normal
Signaling	Notch activation	Akt activation	Akt activation

Table 1: Summary of major features in tumor subtypes related to WHO grades (Phillips et al., 2006).

1.4 New classification of Gliomas

To optimize clinical diagnostics, in 2016 WHO updated glioma classification which was upgrading the name based on histopathological features followed by genetic and molecular criteria such as *IDH*-mutant and *1p/19q*-codeleted. Terms of wildtype use for lacking a genetic mutation in tumors. however, in the unavailability of molecular diagnostic testing or relevant genetic parameter, they labeled NOS (i.e., not otherwise specified) (Louis et al., 2016) (Fig.3).

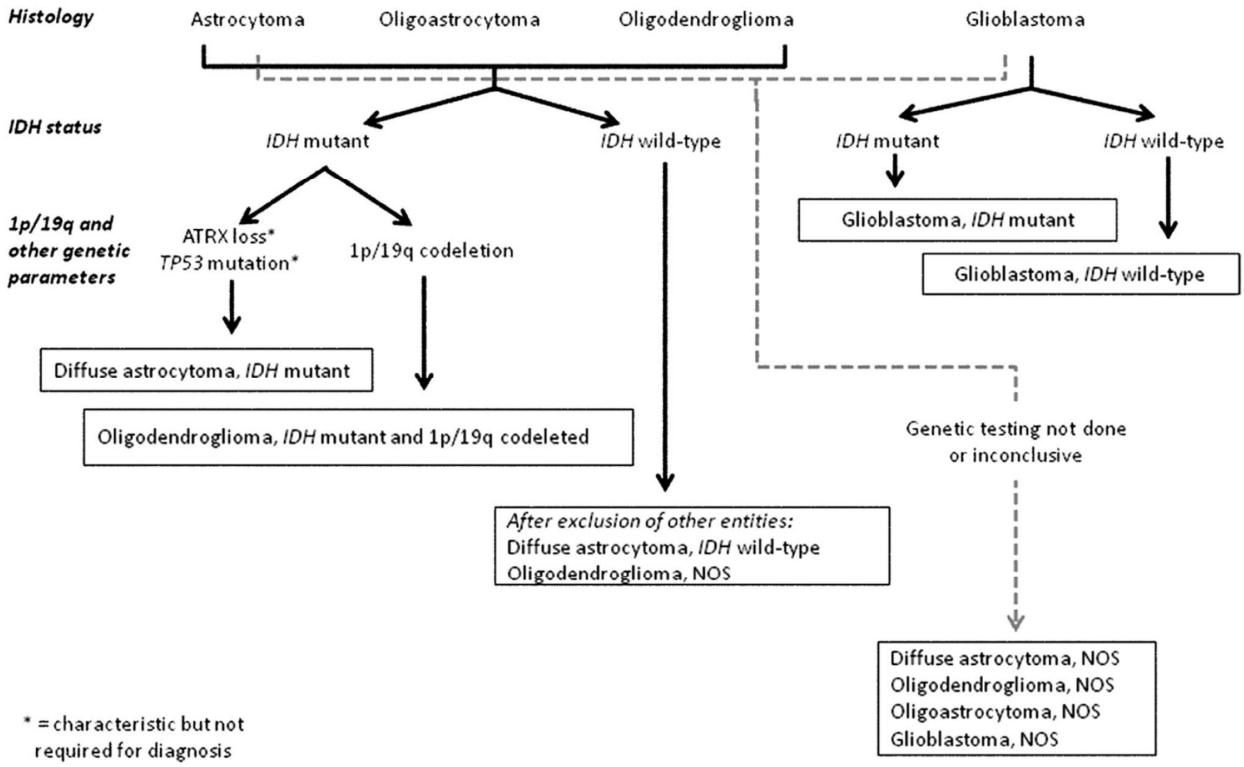

Figure 3: Diagram of new glioma classification based on histological and molecular genetic criteria (Louis et al., 2016).

1.5 ZBTB18

ZBTB18 (ZBTB18/ ZNF238/ RP58) is a transcription factor that belongs to the Broad complex, Tramtrack, Bric à Brac [BTB], or poxvirus and zinc finger [POZ]-zinc finger (BTB/POZ-ZF) family protein and plays a crucial role in brain development and neuronal differentiation (Okado H, 2021, Fedele et al., 2017) (Fig. 4).

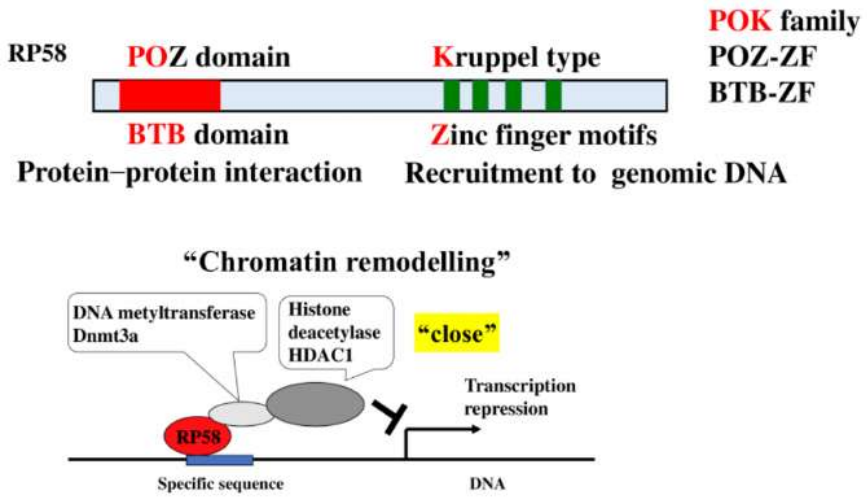

Figure 4: ZBTB18 structure (RP58). RP58 belongs to the POK family (POZ-ZF, BTB-ZF). Lower: Graphical representation of the predicted mechanism of sequence-specific transcription repressor activity. It is shown that RP58 interacts with a DNA methyltransferase in a yeast two-hybrid screen. RP58 is involved in chromatin remodeling by closing the chromatin structure (Okado H, 2021).

Several transcription factors have been known as master regulators of a "mesenchymal gene expression signature" (MGES) in GBM (Carro et al., 2010).

In a survey carried out by Carro and colleagues (Carro et al., 2010), 176 gene expression profile outputs of grade III (anaplastic astrocytoma) and grade IV (GBM) samples were used to construct a transcriptional network by using the ARACNe bioinformatic tools (Basso et al., 2005), which led to the identification of various transcription factors (TFs) that regulate the activation of the "mesenchymal gene expression signature" in GBM. Five of these TFs have been identified as activators (*STAT3*, *C/EBPβ*, *bHLH-B2*, *RUNX1*, and *FOSL2*). Among those,

C/EBPβ and *STAT3* have been characterized as master regulators, sufficient in NSCs and necessary in human glioma cells for mesenchymal transformation. The network also highlighted the ZBTB18 (formerly ZNF238) transcriptional repressor as a potential negative regulator of mesenchymal gene expression signature (MGES) in GBM (Fig. 5).

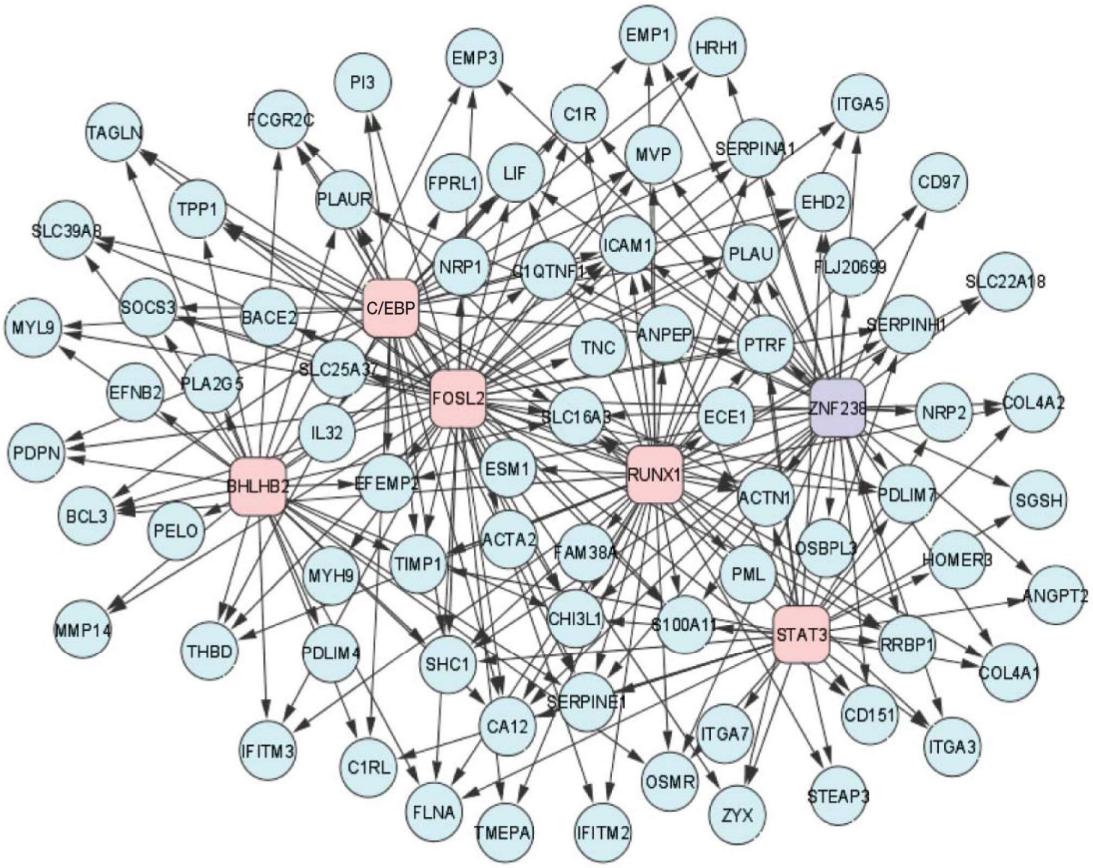

Figure 5: Schematic transcriptional network for High-grade gliomas (HGG): Six TFs control the mesenchymal signature of HGGs. The pink TFs involved in the activation of MGES targets, the purple TFs implicated in repression, and cyan are MGES targets controlled by these TFs. These transcription factors which are interacting with the high-grade glioma mesenchymal signature are identified by using the ARACNe algorithm (Carro et al, 2010).

Previous findings showed that inhibition of ZBTB18 expression in mouse gliomas (GNPs) decreases the expression of the neuronal differentiation markers (*MAP2* and *NeuN*) and downregulates the expression of the cell cycle arrest protein p27, which is a regulator of *GNP* differentiation. ZBTB18 is also downregulated or lost in human GBM cell lines and has been implicated ZBTB18 as a putative tumor suppressor in the brain and impairs tumor formation by counteracting the expression of mesenchymal genes (Tatard VM et al, 2010; Fedele et al., 2017; Xiang et al., 2021). Nonetheless, the exact mechanism of ZBTB18 downregulation in GBM remains to be defined.

Fedele et al, (2017) characterized the ZBTB18 function as a transcriptional repressor of gene signatures; moreover, they identified DNA methylation as a mechanism implicated in ZBTB18 downregulation in GBM. Correlation analysis in 251 GBM samples from the patients of "The Cancer Genome Atlas" (TCGA) indicated a significant inverse correlation between ZBTB18 expression and promoter methylation. This analysis confirmed the role of ZBTB18 as a tumor suppressor in the brain and suggested that it could be silenced by DNA methylation in mesenchymal GBM.

Recently, Ferrarese and colleagues aimed at better defining the mechanism of ZBTB18 function by searching for new ZBTB18 interactors in GBM cells using coimmunoprecipitation (co-IP) and mass spectrometry (MS). They identified *CTBP1/2* as a co-repressor that interact with ZBTB18 in GBM (Ferrarese et al., 2020).

1.6 CTBP

Members of the C-terminal binding proteins (*CTBP1/2*) family mainly function as a transcriptional co-repressor. CTBP family proteins are encoded by *CtBP1* and *CtBP2* paralogous genes in vertebrates. These proteins have similarities in function and structure but also many distinct roles as well. *CTBP1* has 2 splice isoforms, *CtBP1-L* and the shorter form *CtBP1-S*, that splices out exon 1 which encodes the N-terminal 15 amino acids, and is mainly found in the cytoplasm. *CTBP1-S* is also referred to as *CtBP1/BARS* (Brefeldin A-ADP

Ribosylated Substrate), that has been reported to play an important role in the regulation of lipid storage and fission of the Golgi membrane (Dcona et al, 2017).

CTBPs interact with several chromatin regulators such as histone deacetylases 1 and 2, (*HDAC1/2*), the histone demethylase *KDM1A/LSD1*, the histone methyltransferase PRC2, and the chromatin remodeling complexe *NURD*. CTBP proteins control cellular processes not only by acting as transcriptional activators and regulators of the cytoskeleton, but also as transcriptional corepressors which are involved in human cancer by promoting different pro-oncogenic activities such as EMT, migration, cell survival, and invasion (Chinnadurai G, 2002; Ferrarese et al., 2020).

A recent study from the group identified *CTBP1* and *CTBP2* as new ZBTB18 interactors (Ferrarese et al., 2020). The binding is mediated by the VLDLS domain, a CTBP binding motif which is conserved in many proteins and is required for the interactions with *CTBP1/2*. Removal of this motif by site directed mutagenesis (ZBTB18 LDL mutant; ZBTB18-mut), impaired ZBTB18 interaction with CTBP (Fig 6). Phenotypic changes related to ZBTB18 or ZBTB18-mut expression in SNB19 cells showed that ZBTB18 affected cell death, cell proliferation, and migration in accordance with the previous studies (Fedele et al., 2017). ZBTB18-mut seemed to have a mild effect on the proliferation of the cells and on apoptosis while cell migration did not modify (Ferrarese et al., 2020). These pieces of evidence suggested that ZBTB18-driven tumor suppressive function could be both CTBP-dependent and a CTBP-independent (Ferrarese et al., 2020).

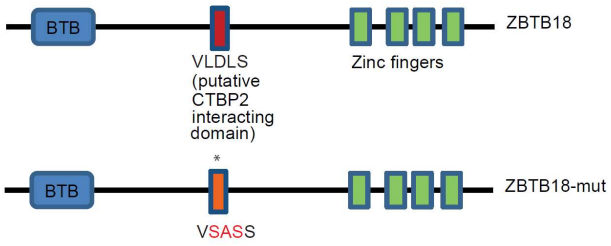

Figure 6: Schematic structure of ZBTB18 protein with BTB and Zinc fingers domain. The putative CTBP2 interacting motif (VLDLS) and corresponding mutation (SAS) are marked (Ferrarese et al, 2020).

1.7 SREBPs

Sterol regulatory element-binding proteins (SREBPs) are transcription factors that can regulate the expression of key enzymes involved in the synthesis of fatty acids, cholesterol, triglycerides, and phospholipids biosynthesis.

Fatty acid synthesis has been shown to play an important role in cancer including glioblastoma. Enhanced lipids accumulated as lipid droplets is a hallmark of cancer cells aggressiveness. Therefore, determining how fatty acid synthesis enzymes are regulated may be helpful from a therapy perspective (Ferrarese et al., 2020).

In mammals, three SREBP proteins have been described: *SREBP-1a*, *SREBP1-c*, and *SREBF2*. The 2 isoforms of *SREBP-1a/c* derive from alternative promoter usage of the *SREBF1* gene (a.k.a. *SREBP1*). *SREBF1* regulates fatty acid synthesis while *SREBF2* is involved in cholesterol production (Horton et al., 2002; Horton et al., 2003).

SREBPs targeted expressions and downstream genes, play an important role in biosynthesis of cholesterol and synthesis of fatty acids such as the encoding genes of fatty acid synthase (*FASN*), stearoyl-CoA desaturase (*SCD*), low density lipoprotein receptor (*LDLR*), glycerol-3-phosphate acyltransferase (*GPAM*), squalene epoxidase (*SQLE*), and lanosterol synthase (*LSS*) (Song et al., 2021; Dorotea et al., 2020; Ferno et al., 2011).A recent study from Carro's group has revealed that ZBTB18 interacts with the cofactors *CTBP1/2* and represses the expression of SREBP genes, involved in de novo lipogenesis.

As mentioned above, *CTBP* is known to be associated with protein complexes containing the histone demethylase *LSD1* (Ferrarese et al., 2020). The proposed model suggests that in absence/low expression of ZBTB18 in GBM, *CTBP* and *LSD1* activate the expression of SREBP genes; however, ZBTB18 expression causes the repression of SREBP genes by inhibiting *CTBP2*-associated complex activity (Ferrarese et al., 2020). Furthermore, it was observed that ZBTB18 expression is accompanied by the reduction of several phospholipid species and decreased lipid droplet content inside the cells, as well as altered metabolic activity (Ferrarese et al., 2020) (Fig. 7).

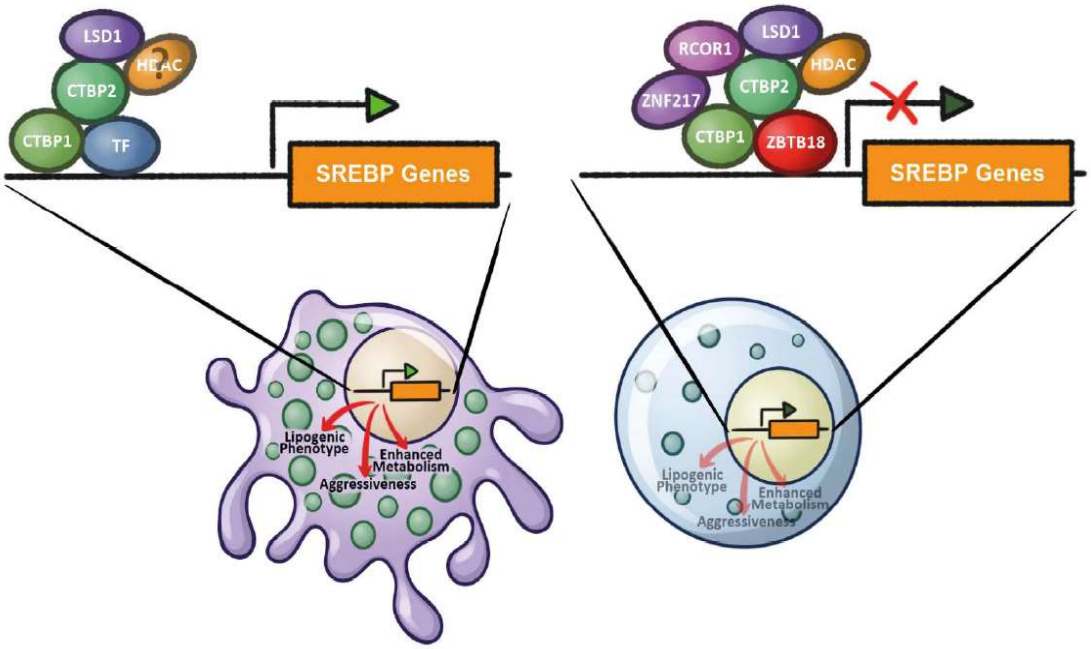

Figure 7: Schematic model of ZBTB18 and its interaction with *CTBP1/2*-mediated regulation of SREBP genes expression and the effects on the cellular phenotype. Complex without ZBTB18 activates the expression of SREBP genes due to *CTBP* and *LSD1* regulations accompanied with other TFs or cofactors (left) while is expressed (right), ZBTB18 plays as an inhibitor and block the *LSD1* demethylase activity and recruits a repressive complex at the promoter of SREBP genes (Ferrarese et al, 2020).

A recent study indicated that *SREBP1* and downstream pathways can be activated by treating cells with oxLDL (Low-Density Lipoprotein from Human Plasma, oxidized) which is known to activate the *SREBP1/2* pathway in both WT and mut models (Schmitt et al., 2021).

Although the exact role of oxLDL in cancer cell metabolism is not completely known, some evidence indicates that oxLDL induces a shift in energy balance. This not only supported by a role for oxLDL in cancer progression but also showed the possibility of targeting oxLDL as a therapeutic choice in cancer (Bitorina et al., 2021).

1.7.1 Lipid droplets (LDs)

Lipid droplets (LDs) are dynamic cytoplasmic organelles which is formed by a neutral lipid core restricted by a monolayer of phospholipids with various proteins (Fig. 8). The size and number of LDs are different based on cell types or between individual cells of a population (Walther.Farse, 2012; Bozza.Viola, 2010).

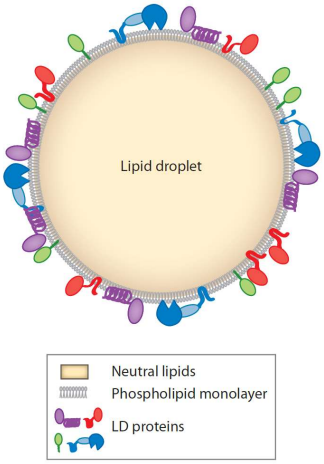

Figure 8: Schematic structure of lipid droplets (LDs) from Walther and Farse, 2012.

Bozza and Viola 2010 showed that numbers of lipid droplets are increased in inflammatory and cancer cells using oxLDL treatment in mouse peritoneal cells (oxLDL-injected mice) as compared to PBS treated cells (PBS-injected mice) (Bozza.Viola 2010).

In 2017 Geng and Guo suggested LDs as novel diagnostic biomarker for GBM, since it is not detectable in normal brain tissues and low-grade gliomas. They reported *SOAT1* (sterol-O transferase 1) function in SREBP regulation since it is a main enzyme implicated in formation of LD in GBM. Reports showed that *SOAT1* inhibition significantly down-regulated SREBP activation and lipogenesis, block cholesterol esterification, and resulting to repress GBM growth and enhance survival in xenograft models via block of *SREBP-1*-regulated lipid synthesis (Geng.Guo 2017; Geng et al., 2016).

1.8 LSD1 and HDAC

Histone acetylation is one of the most well-studied epigenetic modifications which is a process regulated by histone acetyltransferases (HATs) and histone deacetylases (HDACs) (Singh et al, 2011). Of note, histone deacetylase (HDAC) inhibitors lead to de-repression genes that eventually result in growth inhibition, differentiation, and apoptosis of cancer cells (Glaser K. B., 2007).

Although HDAC are mostly known to be involved in transcriptional repression, various studies have shown that HDAC can mediate gene activation in cooperation with *STAT3* (Signal transducer and activator of transcription 3) and *STAT5* (Rascle et al., 2003; Pinz et al., 2015). *STAT3* is one of the crucial transcription factors, which regulates cell migration, proliferation, and differentiation. It is also responsible for angiogenesis, inflammatory response, and programmed cell death and activation of the immune system. Garg et al., discovered that the phenotype of cancer stem cells can be hold by hyperactivation of *STAT3* signalling. This is occurred by metabolism of the cell, modulation of the tumor microenvironment and immune responses in favor of drug resistance and metastasis (Garg et al., 2020).

Previous studies have indicated that genetic and epigenetic mechanisms cause the heterogeneity and dysregulation of various signalling pathways in GBMs. Meanwhile, various epigenetic enzymes have been implicated in the regulation of tumorigenic mechanisms and have become important targets for cancer treatment. The lysine-specific demethylase 1 (*LSD1*) which is also known as *BHC110*, *AOF2*, or *KDM1A* also causes K4 methylation removal from histone H3 (H3K4) demethylation (Singh et al, 2011; Singh et al, 2015). As mentioned above, a previous study from the group has illustrated that ZBTB18 affects CTBP and LSD1 function. Specifically, it was shown that ZBTB18 inhibits LSD1 demethylation activity to block LSD1-mediated activation (Ferrarese R. et al., 2021).

1.9 Epigenetic inhibitors

In cancer and neurodegeneration disease, blocking of HDACs function is important as a therapeutic option. HDACi, vorinostat, has been approved by the FDA (The first US Food and Drug Administration) for the treatment of cutaneous T-cell lymphoma. Thereafter, dozens of other HCDA inhibitors (HDACis) have been developed and tested in various stages of clinical trials. HDACis categories are structurally dissimilar and different at HDACs classes, which include cyclic peptides, hydroxamates, benzamides, aliphatic acids. Using HDAC to treat cancer cells lead to cell growth arrest and cell death; however, the exact mechanisms of action are still unknown (Singh et al, 2011; Singh et al, 2015).

In 2018, Kalin and colleagues reported a synthetic hybrid agent, Corin, which derives from the LSD1 inhibitor (Compound 7) and class I HDAC inhibitor (entinostat) (Fig 9 and 10). Using enzymological analysis, the authors suggested that Corin constantly inhibits the CoREST complex HDAC activity by targeting the CoREST complex, when compared with entinostat. The CoREST complex is a composed by HDAC1 or its close paralog HDAC2, the scaffolding protein CoREST, and lysine specific demethylase 1 (*LSD1*) (Fig 11) (Kalin et al., 2018).

Another recent study revealed that Corin treatment of DIPG (Diffuse intrinsic pontine glioma) cells induced cell death, cell-cycle arrest, and cellular differentiation phenotype. Moreover, it drives transcriptional changes correlating with increased survival time in DIPG patients. Melanoma also was effective in the slowing of tumor growth (Kalin et al., 2018; Anastas et al., 2019).

Taken together these studies indicate that Corin is a bifunctional inhibitor of HDACs and LSD1, which could be useful to target tumor cells in various cancers (Kalin et al., 2018; Anastas et al., 2019).

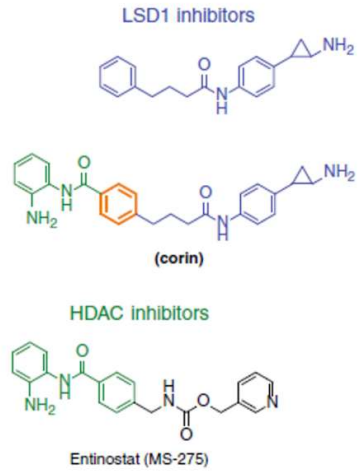

Figure 9: Corin structure compared to LSD1 inhibitor (Compound 7) and HDAC inhibitor (entinostat) modified from Kalin et al., 2018.

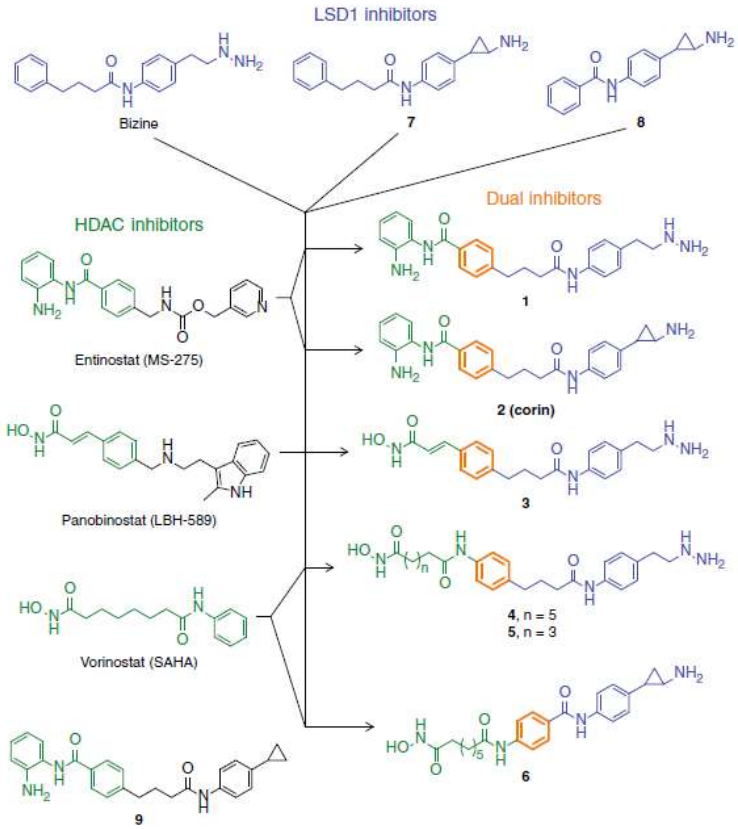

Figure 10: Combination strategy of the pharmacophores of preclinical LSD1 inhibitor and clinically HDAC inhibitors to generate dual action HDAC-LSD1. Blue showed the features of LSD1 inhibitor, Green included HDAC inhibitor features, Orange indicated shared structural features, and Black related to the features that are not incorporated into dual inhibitors (Kalin et al., 2018).

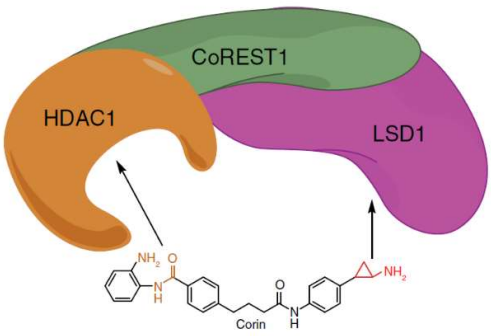

Figure 11: Schematic model showing dual engagement mechanism of Corin leading to maintained inhibition of CoREST complex HDAC activity (Kalin et al., 2018).

2 Objective (Hypothesis and Aims)

A previous study from the group indicates that ZBTB18 plays a tumor suppressive role in GBM by repressing the expression of mesenchymal genes. Furthermore, ZBTB18 induced apoptosis and reduced cell proliferation and invasion (Fedele et al., 2017). More recently, our group has discovered that ZBTB18 causes downregulation of SREBP genes and consequent inhibition of fatty acid synthesis (Ferrarese et al., 2020). To follow up on these studies, in this project, we aimed to understand whether ZBTB18-mediated SREBP genes regulation is important for ZBTB18 tumor suppressor function in glioblastoma. To further study ZBTB18 function in GBM, especially in the context of SREBP gene regulation, we further planned to knock down ZBTB18 by CRISPR/Cas9 mechanism. Specifically, we aimed to study whether ZBTB18 knock down increases the expression of SREBP genes, leads to excess of lipid droplet due to more fatty acid synthesis and metabolism activity. Finally, given the implication of *LSD1* and *HDAC* in SREBP activation, we evaluated the effect of inhibiting HDAC and LSC1 using Corin, which has been shown to act as a dual inhibitor of *HDAC* and *LSD1* activity.

We have planned to address the following specific aims:

I. To investigate the role of SREBP pathway downregulation in ZBTB18-mediated function.
II. To evaluate the effect of knocking down ZBTB18, in the context of SREBP gene regulation.
III. To characterize the use of Corin to inhibit HDAC and LSD1, in the context of SREBP transcriptional regulation.

3 Materials and Methods

3.1 Cell Culture of Brain Tumor Stem-like Cells (BTSCs)

A small population of tumor cells categorized by stem cell properties have been discovered in recent years. In human brain tumors (gliomas), these cells are known as brain tumor stem cells (BTSCs), which contribute to the initiation and development of gliomas (Mao et al., 2009; Hide et al., 2008).

All the BTSC Cell lines in this thesis were derived from primary glioblastoma tissue samples from patients operated on in the neurosurgery department of the Neurocenter, Uniklinik Freiburg, Germany, who provided consent.

3.1.1 BTSC cell culture of patient-derived GBM cell line

Different types of mesenchymal BTSCs were used in this thesis. BTSC168 and BTSC475 cells were grown in adherent plates and BTSC233 sphere cells were cultured in flasks.

All the cells were maintained in CSC medium which was culture serum-free consisting of Neurobasal media supplemented with appropriate growth factor (Table 2). That was monitored and refreshed in adequate number of days (approximately three to four). Around the time of confluence, cells were split and were passage to a new plate or flask by removing the tissue debris and using cell dissociation reagent. The previous culture medium of BTSC168 and BTSC475 cells was aspirated and discarded. Then cells were detached by adding 1mL of non-enzymatic detachment solution and followed by washing with 5 mL phosphate-buffered saline (PBS). The suspension then was transferred into a 15mL falcon and was sedimented by centrifugation at 720 rpm, 5 min, and room temperature. Thereafter, the supernatant was aspirated, the resuspended pellet was taken up added 7mL fresh BTSC medium depending on the size of the cell pellet, and was moved to a new plate. Regarding BTSC233 cells, the procedure was the same, except the sphere cells which first were moved to a 15mL falcon, then were sedimented in the same condition mentioned above. The supernatant then was

aspirated and the cells were separated into a single cell using 200µl of cell dissociation solution and pipetting up and down. The cells then were seeded into a new flask by adding 7ml of fresh medium.

BTSC475 cells which normally expressed ZBTB18 were used for ZBTB18 knockdown by CRISPR/Cas9 technique using "pKLV-U6gRNA(BbsI)-PGKpuro2ABFP" with following selection conditions: Blasticidin (5 µg/ml) and Puromycin (1 µg/ml)

To obtain single clones by limiting dilution, BTSC475 knocked down cells were seeded in 96-well-plate at 1cell/well, grown to confluence and later moved into a 24-well-plate, and subsequently a 6-well-plate to either harvest or freeze a single clone for subsequent experiments.

Table 2: Composition of BTSC medium

Components	**Volume**
Neurobasal medium	50ml
B-27_vitamin A	1ml
N2	500µl
GlutaMax	500µl
FGF basic	20µl
EGF	50µl
LIF	50µl
Heparin	50µl

3.1.2 Cell counting

BTSC cells (168, 475, and 233) were counted to maintain comparable conditions between different experiments. To perform this procedure, non-enzymatic dissociated cells were resuspended in a fresh medium and a 10 µl aliquot was used with the dilution of 1:1 cell culture in Trypan Blue, and were loaded on the Neubauer counting chamber. Then four selected squares on corners covered by the cell suspension were counted and the mean value was calculated using the following formula. Each selected square has an area of 1mm² and a chamber depth of 0.1 mm. Therefore, the calculated number of particles was multiplied by 10^4 to determine the cell amount per 1mL. At the end, the cells were seeded based on the number of cells needed for each experiment.

3.1.3 Cells treatment

Two drugs were used for cell treatment. “OxLDL" (Low Density Lipoprotein from Human Plasma, oxidized) an activator of the SREBP pathway, and “Corin” an inhibitor of LSD1 and HDAC. OxLDL was used at a concentration of 6 µl/mL (according to Thermofisher protocol). For Corin treatment different concentrations (1.0 and 0.5 µM) were used (according to Anastas Cancer Cell 2019). Both treatment drugs were directly added to the medium in a different time course. Specify which control was used.

3.1.4 Transduction of primary GBM cells

BTSC Cells were transduced using concentrated lentiviral stocks of **pCHMWS** (Empty Vector, EV), **pCHMWS**-ZBTB18 and **pCHMWS**-ZBTB18 mutant. Each lentiviral stock was previously tested to determine the amount of virus which yield 100% infected cells. The adherent cells (BTSC168 and BTSC475 cells), were seeded on a 10 cm petri dish (10^6 cells) and allowed to adhere in an incubator for one night. The following day, polybrene was added to the culture medium at the concentration of 2 µl/mL to enhance the transduction efficiency and the cells were infected as follows:

- **pCHMWS EV:** 20 µl for 10^5 cells
- **pCHMWS ZBTB18:** 10 µl for 10^5 cells
- **pCHMWS ZBTB18_mut:** 10 for 10^5 cells

BTSC233, which grows as spheres, where dissociated and immediately transduced and the medium was then replaced 24 hours after the infection.

3.1.5 Cell harvesting

For harvesting cell culture plates, after aspirating the medium, cells were washed two times with ice-cold PBS (1mL in total). The cells, then were collected by scraping and placed into a 1.5mL Eppendorf tube and left in ice. Cells then were centrifuged for 5 minutes at 1000 rpm

at 4°C. The supernatant was discarded and the harvested cell pellets were stored and frozen at -80°C.

3.1.6 Freezing and thawing cells

To freeze, BTSC cells were harvested, centrifuged for 5 minutes at 750 rpm at room temperature. Then cells were dissolved in a 1ml Synth-a-Freeze medium and transferred in a freezing tube. Next, the tubes were incubated in an isopropanol-containing box which was warmed up before at room temperature and were stored at -80°C for one day and were transferred to liquid nitrogen for long-term freezing.

To thaw the cell lines, the frozen tube was taken out of the freeze, then incubated in a 37°C water bath for 1 minute. The cells were then resuspended with the CSC medium in a ratio of 1:5 and seeded on a new plate. The medium was changed on the following day.

3.2 Real-time Quantification (RT-PCR)

3.2.1 Total RNA preparation

Generally, total RNA was prepared from previously collected and frozen cell pellets. Cells were lysed with Triazol and RNA prepared with miRNeasy® Mini Kit following the manufacturer's instructions. At the final step, the elution was performed using 30 µl RNase-free water. The RNA concentration was then measured using a NanoDrop.

3.2.2 Reverse Transcription (cDNA Synthesis)

A reverse transcriptase reaction was performed to obtain the complementary DNA (cDNA) from the isolated total RNA. DNA-RNA hybrid led to create one DNA strand complementary to the RNA strand from the enzyme reverse transcriptase. cDNA was prepared using the Superscript III kit (Thermofisher). Random hexamers acted as unspecific primers which bound to several complementary sites of the target RNA and made a starting point for the reverse

transcriptase Superscript III. The table below showed the components for the cDNA synthesis that were mixed in a microtube, without the master mix, then was placed into the Thermocycler to start the protocol.

Table 3: Composition of RNA mix to be preheated.

Template RNA solution	500 ng total RNA/reaction
10 mM dNTP Mix	1 µl
50 µM Random Hexamers	1 µl
sterile H2O	up to 12 µl

After heating at 65 °C, the machine then was cooled down to 8°C, the program was paused to add 8 µl of the below listed Master-Mix to each sample and gently compounded. Thereafter, the protocol was resumed until the end.

Table 4: Composition of Master-Mix to be added.

10x RT buffer	2 µl
0,1 M DDT	2 µl
50 mM MgCl2	2 µl
RNaseOUT™ Ribonuclease Inhibitor	1 µl
SuperScript™ III Reverse Transcriptase (200 U/µl)	1 µl

The cDNA protocol was followed by 10 minutes primer annealing at 25˚C, then 50 minutes of extraction at 50˚C, followed by a heating step at 85˚C for 15 minutes. At the end, the cDNA samples were stored either at -20 ˚C or used directly for PCR (Table 5)

Table 5: RT-PCR schedule.

Phase	**Time**	**Temperature**
Denaturation	5 min	65 °C
	1 min	8 °C
Annealing Polymerization	10 min	25 °C
Elongation	50 min	50 °C
Inactivation	5 min	85 °C
End	-	8 °C

3.2.3 RT-PCR

After the transcription of the RNA into cDNA was accomplished, the cDNA products were used for a real-time RCR. The total amount of cDNA samples and each target gene (Table 7) were calculated according to the table 6. The following mixture was prepared according to the samples(n=x) and the number of primers (n=y). The total volumes were triplicated due to 3 replicates of qPCR measuring.

Table 6: Composition of cDNA and Primer Mixes.

cDNA Mix (n=x)	Template cDNA	0.5 µl . 3 . x
	sterile water	7.5 µl . 3 . x
Primer Mix (n=y)	1 µM RT-PCR primer (F+R)	1 µl . 3 . y
	SYBR® Green	12.5 µl . 3 . y
	sterile water	3.5 µl . 3 . y

Table 7: Oligonucleotides used in this study

Primers	**Sequence**
18s_F	5‘-CGCCGCTAGAGGTGAAATTC-3‘
18s_R	5‘-CTTTCGCTCTGGTCCGTCTT-3‘
FASN_F	5’-CCGAGACACTCGTGGGCTA-3’
FASN_R	5’-CTTCAGCAGGACATTGATGCC-3’
SCD_F	5‘-TCTAGCTCCTATACCACCACCA-3‘
SCD_R	5‘-TCGTCTCCAACTTATCTCCTCC-3‘
GPAM_F	5’-GATGTAAGCACACAAGTGAGGA-3’
GPAM_R	5’-TCTTTGGGTTTGCGGAATGTT-3’
LDLR_F	5’-TCTGCAACATGGCTAGAGACT-3’
LDLR_R	5’-TCCAAGCATTCGTTGGTCCC-3’
SREBF1_F1	5’-ACAGTGACTTCCCTGGCCTAT-3’
SREBF1_R1	5’-GCATGGACGGGTACATCTTCAA-3’
SREBF2_F2	5’-CTCCATTGACTCTGAGCCAGGA-3’
SREBF2_R2	5’-GAATCCGTGAGCGGTCTACCAT-3’
SQLE_F	5‘-GGCATTGCCACTTTCACCTAT-3‘
SQLE_R	5‘-GGCCTGAGAGAATATCCGAGAAG-3‘
LSS_F	5‘-ACATTGAGGATAAGTCCACCGT-3‘
LSS_R	5‘-TCGTACCAGGTCAGGATCGTC-3‘
Forward (_F), Reverse (_R)	

Then 24 µl of each cDNA Mix was added to 51 µl of each Primers' Mix in a new microtube to achieve the final mixes. In the end, 23 µl of the final mixture was transferred into the wells of 96-well-plate for qPCR in triplicate. Then the qPCR plate was covered and centrifuged at 1000 rpm at room temperature for 2 minutes. Thereafter, the PCR plate was placed in the PCR cycler and processed based on the protocol mentioned in the table below.

Table 8: RT-PCR program using fast cycling condition (total 40 minutes)

Phase	**Time**	**Temperature**	
Denaturation	20 s	95 °C	
Elongation	3 s	95 °C	40 cycles
Annealing	30 s	60 °C	
End	-	8 °C	

Generally, the cDNA template was denatured at 95 °C for 20 s. The two following steps (elongation and annealing) were followed for 40 repeated cycling.

3.2.4 Data analysis using the Comparative Ct Method

The comparative Ct method was applied in this thesis to quantify the target genes expression using 18s as one of the stable endogenous control genes for validation and normalization of mesenchymal gene expression (Ragni et al., 2013; Vandesompele et al., 2002; Bustin et al., 2002). To do so, the average CT value of each target gene was compared to the CT of the Housekeeping gene in a single sample using the below formula:

$$\Delta C_T = C_{T(target\ gene)} - C_{T(18s)}$$

3.3 Purification of DNA

The purification of genomic DNA and total RNA was performed simultaneously from a single sample by using the AllPrep DNA/RNA Mini Kit from Qiagen Quick-Start protocol. The lysate from homogenized cells was first passed through an AllPrep DNA spin column to isolate DNA, then passed through an RNeasy® spin column to isolate RNA. Purified DNA and RNA were finally eluted in 100 µl of Buffer EB and 30 µl of RNase-free water, directly applied onto the spin column membrane respectively and followed centrifugation of the column at 8,000 rpm for 1 min at room temperature. The eluted samples for DNA and RNA were stored at -20°C and -80°C respectively.

3.4 Polymerase Chain Reaction (PCR)

The amplification of genomic DNA was performed by standard PCR using Platinum® Pfx DNA Polymerase which is a highly processive enzyme with fast chain extension capability. First, the following components (Table 9) were mixed in an autoclaved microtube on ice by pipetting up and down. Then they were centrifuged briefly to collect the contents. The samples then were placed in a PCR cycler and processed based on the protocol mentioned in the table below (Table 10). Generally, the genomic DNA was denatured at 95 °C for 20 s. The two following steps (annealing and extension) were run for 30 repeated cycling. At the end, DNA

samples either could be stored at -20°C until use or were used directly for analysis of the products by agarose gel electrophoresis.

Table 9: Composition of DNA mix for PCR

Component	Volume	Final concentration
10X Pfx Amplification Buffer	5 µl	X
10 mM dNTP Mix	1.5 µl	0.3 mM each
Primer Forward (10 µM)	1.5 µl	0.3 µM
Primer Reverse (10 µM)	1.5 µl	0.3 µM
50 mM Mgcl2	1 µl	1 mM
Platinum® Pfx DNA Polymerase	0.5 µl	1.0-2.5 units
10X PCRx Enhancer Solution	As required	0.5X, 1X, 2X, and 3X
Template DNA	2 µl	
sterile H2O	up to 50 µl	

Table 10: PCR program

Phase	Time	Temperature	
Denaturation	20 s	95 °C	
Annealing	30 s	55 °C	30 cycles
Extention	1 min	68 °C	
End	-	4 °C	

3.5 Sanger Sequencing

Amplified genomic DNA by PCR (that were isolated already from the BTSC475 knockdown cells) were sent for Sanger sequencing to determine the nucleic acid sequence using the Eurofins platform. Submitted primers are listed in the table below:

Table 11: Primers used for Sequencing

Primers	Sequence
Seq_F_gZBTB18#5#3#1	5‘-TCCTCTCTCCCCAGGTTATG-3’
Seq_R_gZBTB18#5#3#1	5‘-AGCAGCCACATAGCAGGC-3’
Seq_F_gZBTB18#1#2#4	5‘AAGTCTGCAAAAAGAAGCTGAAAGAGAAAGCCACCACGGAGGC AGACAGCACCAAAAAG-3’
Seq_R_gZBTB18#1#2#4	5‘-CTGAGGGAGGACTCGGTCTT-3’

3.6 Agarose gel electrophoresis

The PCR products were analyzed by gel electrophoresis. A 1% agarose gel was prepared by mixing 1.00gr agarose (SIGMA) to 100ml 1X TAE (Tris-Acetate-EDTA) buffer and was microwave-heated to dissolve the agarose powder. Since the agarose was dissolved, after a few seconds of cooling down, 10µL of 10000X SYBR™ Safe™ DNA Gel Stain (Invitrogen™) was mixed in the warm solution. After solidifying the gel and removing the comb for around

10-15 minutes, the gel was ready to pour into the gel casting tray. The wells then were submerged with TAE buffer. 5µl of each nucleic acid from the BTSC475 clone sample were loaded adding 1µl of Gelpilot loading Dye 5X (Blue) to each sample. Then, 5µl of TrackIt™ 1 Kb Plus DNA Ladder (ThermoFisher scientific™) was used for comparison and the gel was run at 100 V for about 1 hr. Eventually, the DNA band was visible under UV light using Quantity One® 1-D analysis software to capture the digital images.

3.7 Protein lysates preparation and SDS -PAGE

3.7.1 Whole protein extract preparation

Table 12: Composition of buffers used for cell lysis (Total protein extraction)

RIPA buffer	150 mM NaCl, 50 mM Tris-HCl (pH 7,5), 1 mM EDTA, 1% Igepal, 0,5 % Sodium Deoxycholate, 0,05 % SDS
Adding freshly	1x PMSF, 1x Protease and Phosphatase Inhibitor

To extract proteins, frozen cell pellets were kept in ice and immediately resuspended in RIPA buffer at a 1:1 volume ratio. The mixture was incubated for 30 min on ice within 2 vortex steps every 15 min. Subsequently, lysates were centrifuged at full speed (16,000 rpm) for 30 min at 4 °C. Then within a short time, protein concentration was measured for each lysate and prepared to use on SDS gel.

3.7.2 Cell lysis: nuclear extraction (Histone)

Table 13: Composition of buffers used for cell lysis (Nuclear protein extraction)

TEB buffer:	0,5 % Triton X 100 (v/v), 0,02 % (w/v) NaN3 in PBS
Adding freshly	2mM PMSF

For nuclear protein extract preparation, frozen cell pellets were mixed with the appropriate volume of TEB buffer (1mL TEB buffer per 10^7 cells). The mixture was incubated for 10 min on ice with gentle stirring. Subsequently, lysates were centrifuged at 2,000 rpm for 10 min at 4 °C to recover the cytoplasmic fraction. After spinning down the nuclei and removing the supernatant, the samples were washed with TEB buffer (2 mL TEB buffer per 10^7 cells) and centrifuged like before. Thereafter, the pellets were resuspended in 250 µl 0.2M HCL per 10^7

cells. For acid extraction of histones, pellets were moved to 4 °C overnight in spinning conditions. Then pellet debris was spun down. For neutralizing the PH, 12,5µl 4M NaOH per 10^7 cells were supplemented to the supernatant containing the histones. Then, protein concentration was measured for each lysate and prepared to apply on SDS gel. Nuclear proteins (NPs) were shown to comprise about 10–20% of the total cellular proteins (Narula et al., 2013).

3.7.3 Bradford-Assay

A protein determination method according to the Bradford protocol was used to quantify total protein concentration. This method included binding of Coomassie Brilliant Blue G-250 as a dye to the protein which causes a shift in the absorption maximum of the dye from 465 to 595 nm and makes it turn to blue. This assay is very reproducible and rapid with the dye-binding process virtually complete in approximately 2 min with good color stability for 1 hr (Bradford, 1976). To measure each protein sample, a 1:5 dilution of Protein Assay Dye Reagent Concentrate in ddH2O was prepared in a cuvette. Later on, 1µl of each cell lysate was added with 1mL of the prepared Bradford solution. For the blank, 1µl RIPA buffer was used instead. The protein concentrations were calculated by measuring the absorption at 595 nm with NanoDrop™ 2000c.

3.7.4 Protein samples preparation

For each sample (remaining supernatant) an equal volume 2x Laemmli sample buffer was added. Based on the calculated concentration, each sample was diluted to the lowest concentration by adding 1x Laemmli sample buffer. To denaturation the proteins, samples boiled at 95°C for 5 min. The samples were ready to be used on to the gel after a short centrifugation step.

Table 24: Composition of buffers used for sample preparation.

2x Laemmli buffer	4 % SDS, 20 % Glycerol, 125 mM Tris-HCl (pH 6,8), 1,4 M Mercaptoethanol, few grains Bromphenol blue

3.7.5 Acrylamide gel preparation

The method of Sodium dodecyl sulfate-polyacrylamide gel electrophoresis (SDS-PAGE) is used to separate proteins with a relative molecular mass not smaller than 10 KD with an electric field (Laemmli, 1970; He F, 2011).

Table 35: Composition of stacking and resolving gels as well as buffers as used for the SDS-PAGE.

1x Running buffer	25 mM Tris Base, 250 mM Glycine, 1,7 mM SDS 10x APS: 440 mM Ammonium persulfate
4 % Stacking gel	0.125 M Tris-HCl (pH 6.8), 1 % SDS, 4 % Acrylamide/Bisacrylamide, 0.5 % 10x APS, 0.1 % TEMED
10% Running gel	375 mM Tris-HCl (pH 8.8), 1 % SDS, 10 % Acrylamide/Bisacrylamide, 0.1 % 10x APS, 0.04 % TEMED
17% Running gel	375 mM Tris-HCl (pH 8.8), 1 % SDS, 17 % Acrylamide/Bisacrylamide, 0.1 % 10x APS, 0.04 % TEMED

Based on the table above, the mixture of components was prepared. Tris-HCl buffer was used to adjust the pH value of the stacking and running gel. The ammonium peroxodisulfate (APS) and Tetramethylethylene diamine (TEMED) were added at the end as a chain initiator and polymerization catalyzer respectively to obtain the reaction going. Gels were cast in two steps: first, the running gel compounds were mixed and poured into a gel caster system (BioRad). The gel surface was smoothened by covering it with autoclaved water. After gel formation, the water was discarded and the gel was covered by the stacking gel and a comb was inserted to achieve gel pockets. Hardened gels were either immediately used for gel electrophoresis or stored in wet tissue at 4 °C just for a few days.

Once the gel was ready, 5 µl of the Precision Plus Protein™ WesternC™ Standard applied to one of the gel pockets as a marker to determine the molecular weight of the samples and the remaining ones were filled up between 5-50 µg of the respective samples according to the type of the protein extracts (nuclear extracts or whole protein extract). For each sample, the volume was adjusted using 1x Laemmli to load equal volume in every lane of the gel. Then the gel electrophoresis was run in running buffer around 1-2 hr at 80-120 V, 400 mA, or at least until to see the tracking dye bromophenol blue consisted in the Laemmli buffer had exited the polyacrylamide gel.

3.8 Western blotting

In this step, as an initial part of western blot or Immunoblotting, the macromolecules separated by gel electrophoresis were transferred onto a nitrocellulose membrane to quantify the protein expression levels.

3.8.1 Blotting

Table 46: Composition of buffers used for Western Blotting.

Transfer buffer (> MW)	5 M Methanol, 25 mM Tris, 200 mM Glycine, 1 mM SDS
Transfer buffer (< MW)	5 M Methanol, 25 mM Tris, 200 mM Glycine

In this step by using a wet blotting procedure, proteins were transferred from the SDS gel to nitrocellulose membranes. Thus, the nitrocellulose, two fiber pads, and four sheets of pre-cut blotting filter paper were first moistened in 1x Transfer buffer. The order was first the Black side of the cassette holder down, second the pre-wetted fiber pad, third the two filter papers with formed air bubbles removed, fourth the equilibrated gel which was placed onto the filter paper, fifth moistened nitrocellulose on the gel without air bubbles, sixth the remaining wetted two filter paper with formed air bubbles removed, and finally a fiber pad. At the end after all set in, the cassette was put into the blotting chamber with a consideration of the corresponding direction and filled up by 1x transfer buffer. Electro blotting was performed by applying 400 mA for about 70 min to 1,5 h. The proteins, which had a negative charge due to SDS treatment, were pulled toward the nitrocellulose near the anode side of the blotting chamber.

3.8.2 Blocking

Table 57: Composition of the buffer used for blocking the membrane.

Blocking buffer	5 % (w/v) nonfat milk powder in 0,1% TBST (Washing buffer)

To avoid the binding of unspecific antibodies on the membrane, nonspecific sites were blocked. Thus, the membrane was incubated in prepared fresh milk as a blocking buffer on a platform shaker for 1 hr at room temperature.

3.8.3 Staining with 1st antibody and washing steps

Table 68: Composition of buffers used for washing the membrane.

Washing buffer	50 mM Tris-HCl (pH 7,4), 150 mM NaCl, 0,1 % (v/v) Tween20

The next step to visualize the specific proteins was to block the membrane with appropriate dilutions of primary antibody (Table 19) in blocking buffer overnight at 4°C in a cold room on a rocker. Consequently, to remove unbounded antibodies, three 20 min washing steps were managed using washing buffer. Thereafter, the membrane was incubated with the recommended dilution of conjugated secondary antibody (1 µl) and Precision Protein StrepTactin-HRP (1 µl) in blocking buffer (Table 17) for 1 hr at room temperature. This step was performed by washing the membrane of the immunoblot again thrice.

Table 79: Antibody used in this study

Antibody	Antibody	Host	Dilution	Manufacturer
First antibody	α-ZNF 238 (ZBTB18)	Rb, polyclonal	1:1,000	Abcam
	H3K4me2 (#9725)	Rb, monoclonal	1:1,000	Cell Signaling Technology
	H3K9me2 (#ab1220)	Ms, monoclonal	1:1,000	Abcam
	H3K27me3 (Cat#39055)	Rb, polyclonal	1:1,000	Active Motif
	H3K9ac (#ab4441)	Rb, polyclonal	1:1,000	Abcam
Secondary antibody	Anti-rb-HRP (#NA834V)	Polyclonal Donkey Anti-Rb IgG(HRP)	1:5,000	GE Healthcare
	Anti-ms-HRP (#NA931V)	Polyclonal Sheep Anti-Ms IgG(HRP)	2:5,000	GE Healthcare
Control antibody	Histone 3 (#ab1791)	Rb, polyclonal	1:1,000	Abcam
	α-Tubulin (#ab7291)	Ms, monoclonal	1:10,000	Abcam

Ms: Mouse, Rb: Rabbit, HRP: horse reddish peroxidase, IgG: Immunoglobulin G

3.8.4 Signal development

Clarity™ Western ECL Substrate has Detection reagent/Substrate solution which both are helped for densitometric quantification. The reporter enzyme horse reddish peroxidase (HRP), which is capable to cleave a chemiluminescent substrate in the presence of peroxide is linked to the secondary antibody. Light generation is a consequence of catalyzation due to luminol oxidation. To develop it, the membrane in the first step was dripped off on paper, then placed

onto a clear film. 2 ml of the 1:1 ECL Detection reagent/Substrate solution mixture which has immediately coated the membrane and then was incubated for 2-3 min at room temperature in the dark. In the next step, after removing the reagent from the membrane and covering it with transparent plastic wrap without air bubbles, the luminescent signal was capable of being detected by Molecular Imager ChemiDoc™ XRS+ acquiring images. The produced light is equal to the amount of target protein on the nitrocellulose; therefore, the relative expression of tested target proteins could be measured by western blotting.

3.8.5 Re-incubation with different antibody

In case of using an already developed membrane for the detection of another protein, the membrane was again incubated with blocking buffer for 1 hr at room temperature. Subsequently, another primary antibody was used according to the above-mentioned protocol.

3.9 Lipid staining using Bodipy

To assess the accumulation of lipids in the cells, BTSC475 cells were plated in 4-well chamber slides which were laminated before seeding at a density of 2×10^4 cells/well in 500 µl per well medium. The cells then were incubated overnight at 37℃, 5% CO_2. On the following day, slides were then washed with 500 µl per well PBS after discarding the medium. The cells were then fixed with 4% paraformaldehyde in PBS for 15 min at room temperature in the dark and processed for the staining after being briefly washed with PBS. Lipid droplets were stained with 0.5 µg/ml Bodipy TMR-X SE (Thermo Fisher Scientific) in 150 mM NaCl for 10 minutes at room temperature. Nuclei were counterstained with 4′,6-diamidino-2-phenylindole (DAPI, Sigma-Aldrich). The slides then were incubated in dark for 30 min at room temperature, washed with sterile water, and fixed with a coverslip using a mounting medium. Pictures were acquired 1 h after drying the slides at room temperature using FSL confocal microscope (Olympus).

3.10 Metabolic assay

To investigate ATP production rate, Metabolic assays were performed using Agilent Seahorse XF Real-Time ATP Rate Assay Kit Oxygen consumption rate (OCR) and extracellular acidification rate (ECAR) were measured using the Seahorse XFe 96 Extraflux Analyzer (Agilent Technologies, Lexington, MA) to evaluate the metabolic profile of BTSC475 cells. The assays were continued based on the manufacturer's instructions. Briefly, the cells (EV or ZBTB18 knockdown and those treated with Corin which were cultured already in normal medium for 48 hours) were plated at a density of 75,000 cells/well and remained to adhere overnight at 37℃, 5% CO2. The following day, first the medium was changed over to Seahorse XF DMEM base medium, without phenol red (Agilent) supplemented with 2 mM Glutamine, 10 mM Glucose, and 1 mM Sodium Pyruvate pH 7.4. The metabolic modulators were counted using an ATP production rate assay kit by registering the basal measurement of OCR and ECAR for each condition and then the values after adding 0.5 µM rotenone/antimycin A (final) and 1.5 µM oligomycin (final concentration). Finally, the total ATP production rate and also both ATP production rate from glycolysis and mitochondrial respiration were calculated separately by the below formula:

Glycolysis:
glycoATP Production Rate (pmol ATP/min) = glycoPER (pmol H^+/min)

Mitochondrial respiration:
1) OCR_{ATP} (pmol O_2/min) = OCR (pmol O_2/min) - $OCR_{Oligomycin}$ (pmol O_2/min)
2) mitoATP Production Rate (pmol ATP/min) = OCR_{ATP} (pmol O2/min) * 2 (pmolO/pmol O_2) * P/O (pmolATP/pmol O)

Total ATP production:
ATP Production Rate (pmol ATP/min) = glycoATP Production Rate (pmolATP/min) + mitoATP Production Rate (pmol ATP/min)

3.11 Apoptosis assay

Transduced BTSC168 and BTSC233 cells were counted for a density of $1x10^3$ per well and seeded in a 96 well plate (dark plate). Then they moved to the incubator (37℃, 5% CO2)

overnight. The following day caspases 3 and 7 activity was measured using the Caspase-Glo® 3/7 Assay (Promega; protocol have been provided by the manufacturer), and by Infinite 200 PRO which is an easy-to-use multimode plate reader.

3.12 EdU proliferation assay

The cell proliferation rate was assessed by measuring 5-Ethynyl-2′-deoxyuridine (EdU) incorporation in replicating cells. BTSC168 and 233 cells were plated in 4-well chamber slides which were laminated (1000:10; final dilution of 50 µl laminin in 5ml PBS) before seeding and incubated at room temperature under the bench for 4 hr. The cells then were seeded at a density of 2×10^4cells/well in 1ml per well medium and incubated overnight at 37℃, 5% CO_2. In the following day, half of the medium from the slides was changed over to EdU reagent diluted (2:1000; 1µl EdU in 500 µl BTSC medium per well) and incubated 4-6 hr at 37℃, 5% CO_2. The medium containing EdU was then discarded and the slides were fixed with 4% paraformaldehyde in PBS for 15 min at room temperature in the dark and incubated overnight at 4℃ with PBS. Afterward, slides were rinsed with 1ml 0.5% Triton x-100 in PBS for 20 min at room temperature and also were washed twice with 1ml 3% BSA in PBS respectively. Then, the slides were incubated for 30 min at room temperature in the dark with 200 µl of EdU master mix. The EdU master mix was prepared as follows:

Table 20: EdU detection Master mix

Component	Volume
dH2O	151.6 µl
Reaction Buffer (Orange 4℃)	20 µl
Catalyst (Green RT)	8 µl
5/6SR101-PEG3-Axle(Red20℃)	0.4 µl
Buffer Additive (Blue20℃)	20 µl

The slides were then washed with 1ml 3% BSA in PBS, once with 1ml PBS, and once with 1ml dH_2O. Cells were counterstained with DAPI and mounted with a coverslip using a mounting medium (Dako Fluorescent mounting medium). Images were then captured using FSL confocal microscope (Olympus).

3.13 Invasion assay

The rate of invasive GBM cells was assessed using chamber slides (Corning® BioCoat™ Matrigel® Invasion Chamber). The invasion chambers (24 inserts each) were removed from -20°C storage freeze and allowed to equilibrate to room temperature. The chambers were the rehydrated by adding 500µl of warm (37℃) Neurobasal (bicarbonate-based culture medium) to the bottom of empty wells. The inserts were then transferred to Neurobasal by sterile forceps and the interior of the inserts was filled with the same amount (500µl) of Neurobasal). The invasion chambers were then incubated at 37℃, 5% CO_2 for 2 hours. After rehydration, the medium was carefully removed without hurting the membrane. Then 750 µl of BTSC medium containing PDGF as chemoattractant (1000:0.2; final concentration of 4µl PDGF in 20ml BTSC medium) were added to the bottom of empty wells. The inserts were then moved to the PDGF-containing medium avoiding air bubbles trapped beneath the membranes. Afterwards, BTSC168 and BTSC233 cells were seeded in the interior of inserts (one chamber for the control and one for the treated cells by oxLDL) with a density of 2.5×10^4 cells/well in 500 µl Neurobasal medium and incubated at 37℃, 5% CO_2 for 22 hours. Then, to measure cell invasion, the suspension cells from the inserts were aspirated and non-invading cells from the upper surface of the membrane were removed by “scrubbing”. The staining step was then performed by washing the wells with500 µl/well PBS and then adding 500 µl/well fixative solution for 15 min at room temperature. After the fixation, PBS was discarded, and the well were washed with 500 µl/well of distilled water. After that, 500 µl/well 1% crystal violet was added to stain to the wells as long as starting washing steps with water and mounting the membranes. The wells were then abundantly rinsed with water. To count the invading cells, the membrane was removed from the inserts by cutting through the membrane edge with a sharp scalpel blade. and the membranes were then mounted with a coverslip and images were acquired by Light Microscopes imaging using ZEISS Axio Imager 2 equipped with software ZEN 2.6 (blue edition). The total number of cells was counted in several fields of membranes.

4 Results

4.1 Effect of ZBTB18 on lipogenic gene expression in BTSC168 and 233 cell lines after treatment with oxLDL

A Previous study (Fedele et al., 2017) showed that ZBTB18 as a tumor suppressor function induces apoptosis and reduces cell proliferation and invasion. More recently, it was demonstrated that ZBTB18 regulates the expression of SREBP genes involved in fatty acid synthesis (Ferrarese et al., 2020). Hence, we hypothesized that SREBP could be implicated in this circumstance. Therefore, we planned to activate SREBP again and to investigate whether the activation of SREBP could reduce the effect of ZBTB18 on cell invasion, proliferation, and apoptosis. Therefore, we expected to observe an enhancement in cell proliferation and invasion and a decrease in apoptosis.

SREBP1 and the downstream pathway can be activated by treating cells with oxLDL which activates the SREBP1/2 (Schmitt et al., 2021). In order to establish the best condition to induce SREBP genes, a time course treatment with oxLDL in 2 different BTSCs (168 & 233) was set up. OxLDL has been previously shown to induce upregulation of the SREBP pathway (Schmitt et al., 2021). Cells were treated with oxLDL (6 µl/ml) and harvested at 3,5 and 7 days after treatment.

To select the most suitable housekeeping gene, we examined multiple HK genes (18s, TBP, ACTIN, and GAPDH) by qPCR and identified 18s as the most effective (data not shown).

The qPCR result showed a gradual reduction in all targets expression in BTSC168 cells throughout 7-days oxLDL treatment. Instead, in BTSC233 cells all SREBP genes showed a considerable enhancement compared to the control. Data showed that the majority of the selected targets were upregulated after 5-days of oxLDL treatment (Fig. 12A).

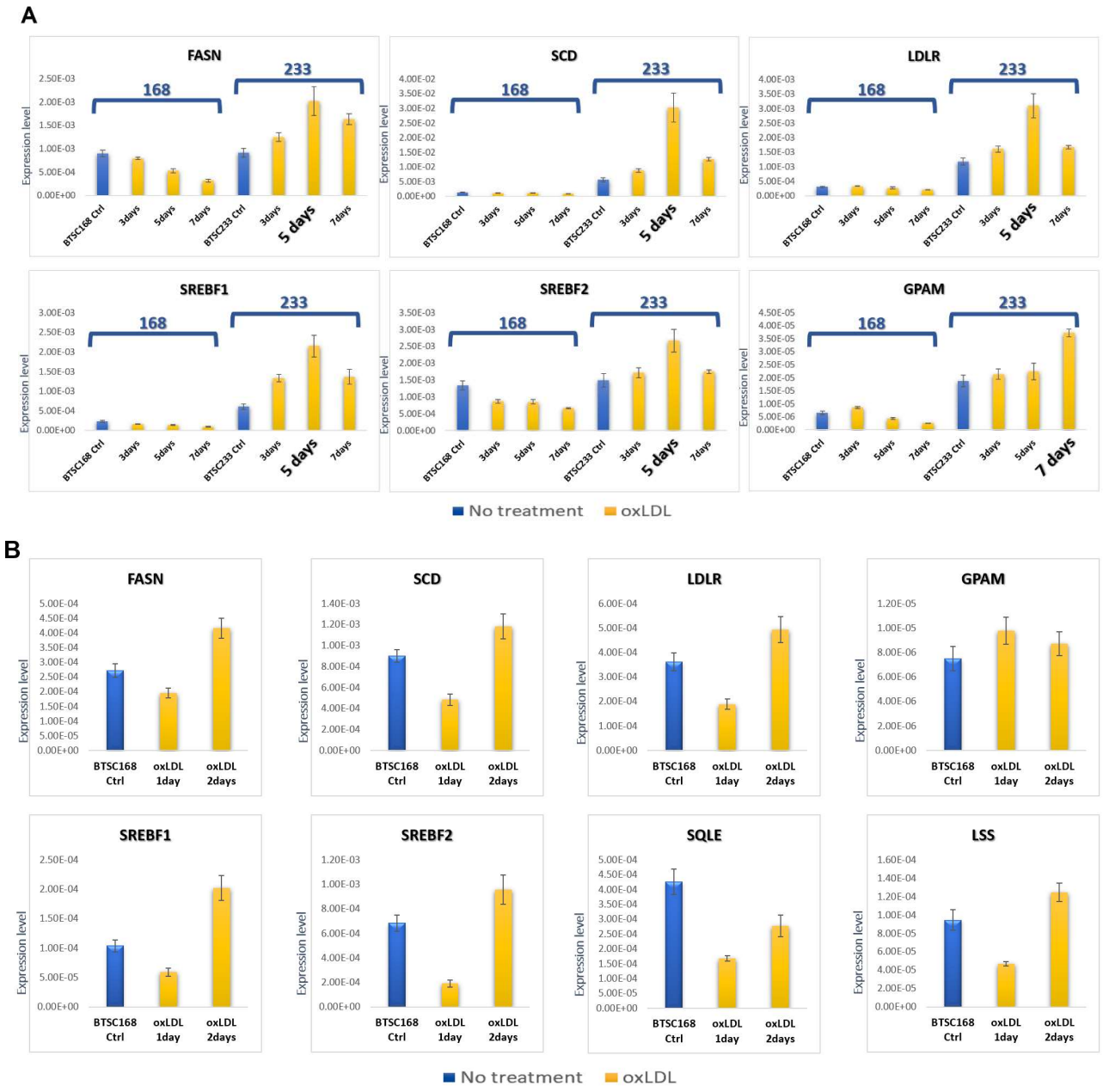

Figure 12: qPCR analysis of selected SREBP genes in BTSC168 and 233 treated with oxLDL for the indicated time points. The average and standard deviation refer to 3 technical replicates. A.Gene expression in BTSC233 showed an increase after 5 days compared to the other conditions. B. BTSC168 showed upregulation of the genes 2 days after treatment.

To find out more specific treatment conditions for BTSC168 cells, available BTSC168 cells previously transduced with Empty vector (EV) were selected and treated with oxLDL. The result from qPCR indicated some relative reduction after 24 hours while showing a considerable raise of all the target genes after 48 hours of treatment (Fig.12B). Table number 21 shows the total of targets related to time-course treatment with oxLDL in both cell lines 168 and 233.

SREBP genes	Ctrl	oxLDL treatment						
	No treat	2 Days	3 Days		5 Days		7 Days	
		168	168	233	168	233	168	233
FASN		*				*		
SCD		*				*		
LDLR		*				*		
GPAM		*						*
SREBF1		*				*		
SREBF2		*				*		
LSS		*				-		
SQLE		*				-		

Table 21: qPCR results in different conditions treating with oxLDL (BTSC168, BTSC233) related to the various SREBP target genes.

To characterize the ZBTB18 function in the expression of lipogenic genes, the cell lines BTSC168 and BTSC233 were transduced with concentrated pCHMWS lentiviral stocks of Empty vector (EV), ZBTB18, and ZBTB18 mutated gene transcript due to the lack of native ZBTB18 expression in the selected cell lines.

To compare the effect of ZBTB18 overexpression before and after treatment, different time points were set up in the two selected cell lines. BTSC168 were infected with EV, ZBTB18, and ZBTB18_mut on day zero and subsequently treated with oxLDL on day two for 48 hours. In BTSC233 cells were treated with oxLDL first and then transduced with EV, ZBTB18, and ZBTB18_mut.

To confirm the overexpression of ZBTB18 and ZBTB18_mut, western blot was performed using whole protein lysates from the harvested pellets (Fig. 13A,B). ZBTB18 and ZBTB18_mut appeared to be overexpressed while no ZBTB18 was detected in both cell lines infected with the empty vector (EV). BTSC168 showed a successful overexpression in ZBTB18 where ZBTB18_mut was expressed at a lower level.

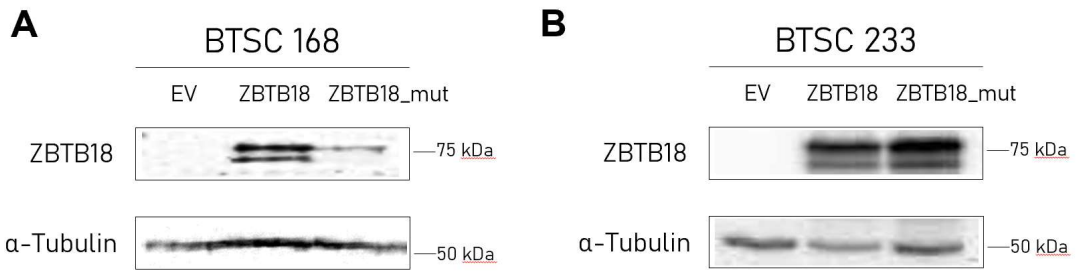

Figure 13: Western blot analysis of EV, ZBTB18, and ZBTB18_mut expression in BTSC168 and BTSC233 cells using anti-ZBTB18 antibody and normalized with α-Tubulin. Both cells expressed the ectopic ZBTB18 or ZBTB18-mut while no endogenous ZBTB18 was detected in EV.

Analysis of three independent qRT-PCR experiments of BTSC168 showed an overall decrease in the expression of the selected SREBP targets in the cells treated with oxLDL as compared to the control, differently from what we expected based on the known oxLDL role and our preliminary set up experiments. Moreover, almost no effect due to ZBTB18 expression (downregulation of SREBP genes in the ZBTB18 overexpressing cells compared to the EV) was observed (Fig. 14A).

Similarly, qPCR analysis of BTSC233 cells transduced with ZBTB18 and ZBTB18-mut did not show a statistically significant change in the expression of the tested SREBP genes. Among the tested targets, ZBTB18 tended to repress *SCD, SREBF1* and *LDLR* although the results did not appear significant (Fig. 14B). Therefore, these experiments remain unconclusive and needs to be repeated.

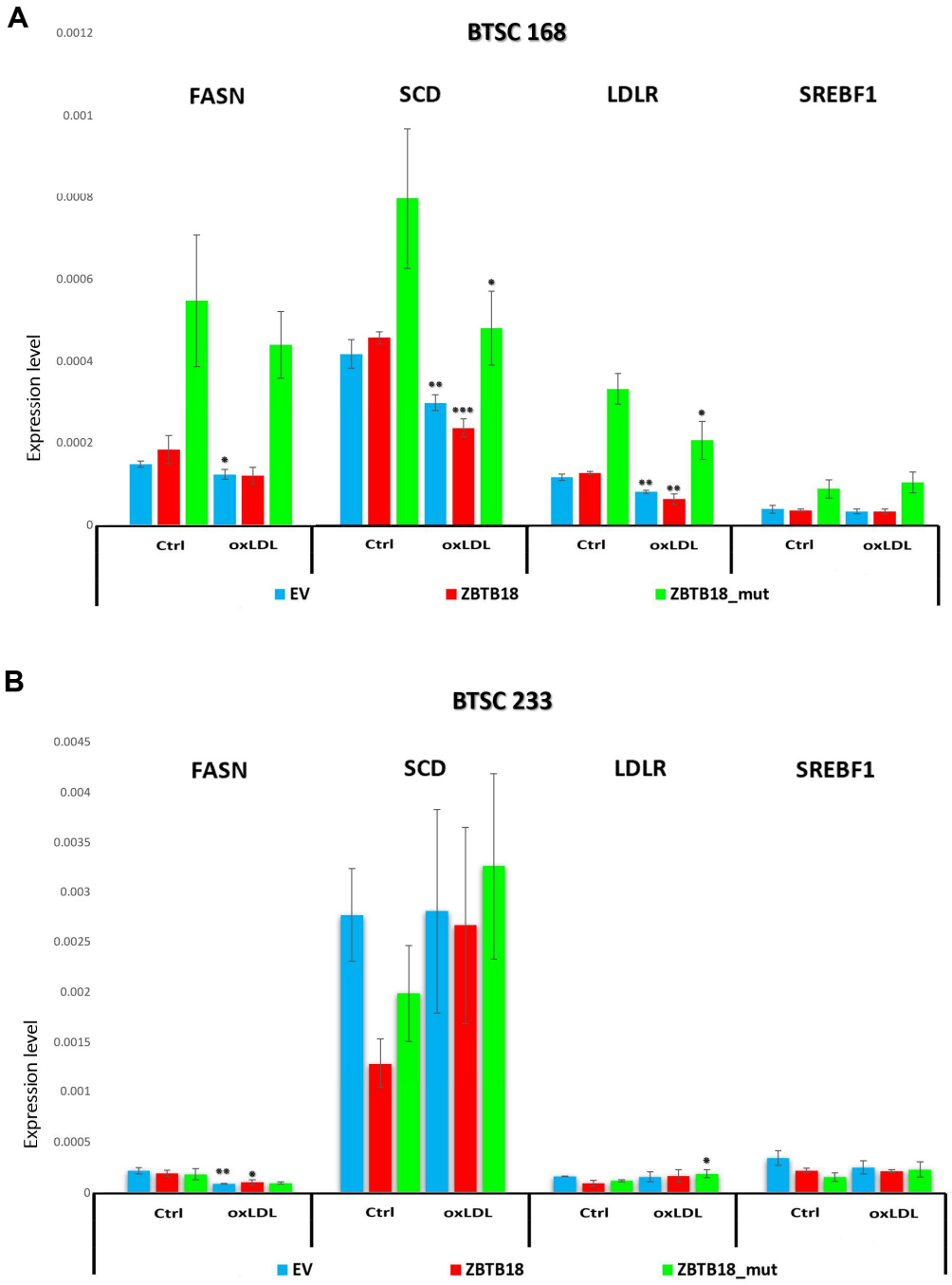

Figure 14: qPCR analysis of SREBP genes in BTSC168 and 233 cells transduced EV, ZBTB18, and ZBTB18_mut treated with oxLDL. A. In BTSC168 cells, overall reduction was observed in the selected genes while no increase was caused by oxLDL treatment. B. In BTSC233 cells, ZBTB18 tended to cause downregulation of some SREBP genes; however, no effect by oxLDL treatment was observed. The average and standard deviation refer to 3 technical replicates. n=3; error bars ± s.d. *p < 0.05, **p <0.01, ***p < 0.001

4.2 Effect of ZBTB18 on phenotypic changes in BTSC168 and 233 cell lines after treatment with oxLDL

To assess phenotypic alterations, investigation associated with ZBTB18 or ZBTB18-mut expressions in BTSC168 and BTSC233 cells was accomplished in parallel with the level of gene expression.

Apoptosis assay was performed with both cell lines upon seeding the cells in a 96 well (dark plate) using the previously established conditions for oxLDL treatment (Fig 15A,B). The results in BTSC168 and BTSC233 cell lines, showed that apoptosis was increased as expected when ZBTB18 was expressed. Plain cells treated with or without VP16 (to induce apoptosis) were applied as a control. In BTSC168 cells, no change in apoptosis was observed between cells transduced with EV treated with or without oxLDL. However, since oxLDL treatment did not show an effect at the level of gene expression in both cell lines, no changes in the cells treated with oxLDL could be related to the oxLDL effect on cell death (Fig. 15A,B).

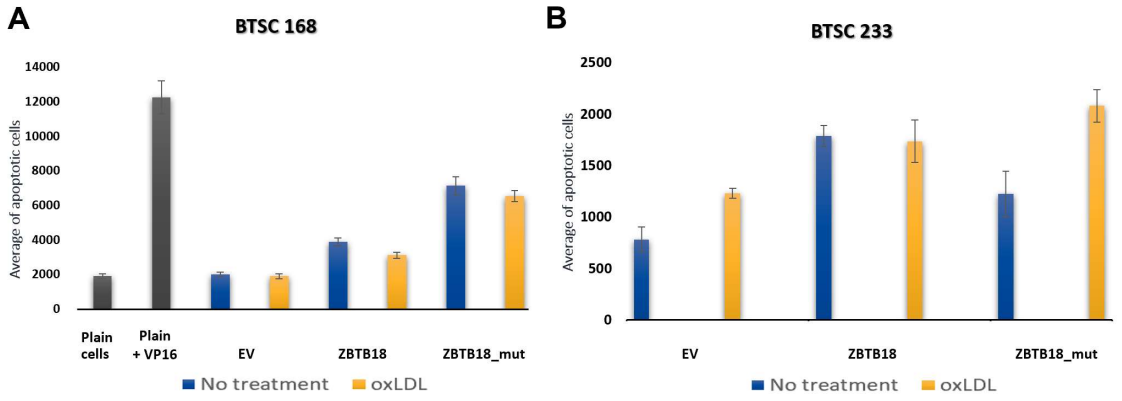

Figure 15: A. B. Apoptosis assay analysis of transduced BTSC168 (a) and 233 (b) treated with oxLDL. The average and standard deviation refer to 3 technical replicates. VP16 was used to induce apoptosis in the plain cells as a control. The level of apoptosis showed higher in cells transduced with ZBTB18 compared to EV no matter what oxLDL did in tested cells.

Measurement of cell proliferation by EdU assay indicated that no considerable change occurred upon oxLDL treatment in cells transduced with EV. The proliferation rate of ZBTB18

and ZBTB18_mut transduced BTSC233 cells appeared to be reduced as compared to the control (Fig. 16A,B).

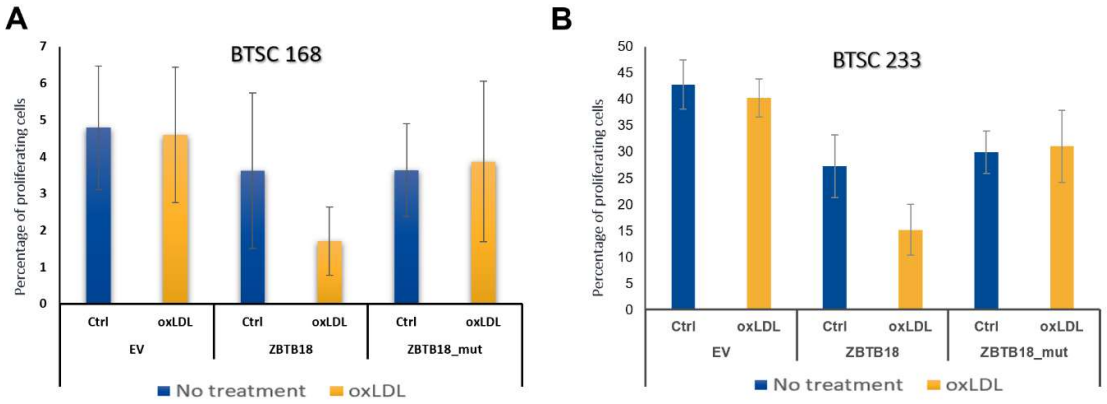

Figure 16: EdU assay analysis of transduced BTSC168 (A) and 233 (B) treated with oxLDL. The average and standard deviation refer to 2 technical replicates. The treated cells were less proliferating.

Finally, we measured the effect of oxLDL on ZBTB18 effect on cell invasion. Invasion assay analysis illustrated that the number of invasive cells was decreased in transduced BTSC233 treated with oxLDL. As expected, we could observe fewer invading cells in the ZBTB18 and ZBTB18_mut compared to the EV. Data showed a reduction in ZBTB18 cells compared to the EV due to reduced migration. The ZBTB18_mut also showed a reduction compared to the EV. This observation confirmed that in the presence of ZBTB18, cell proliferation was reduced; however, oxLDL did not seem to have, consistent with the lack of effect at the level of gene expression (Fig. 17).

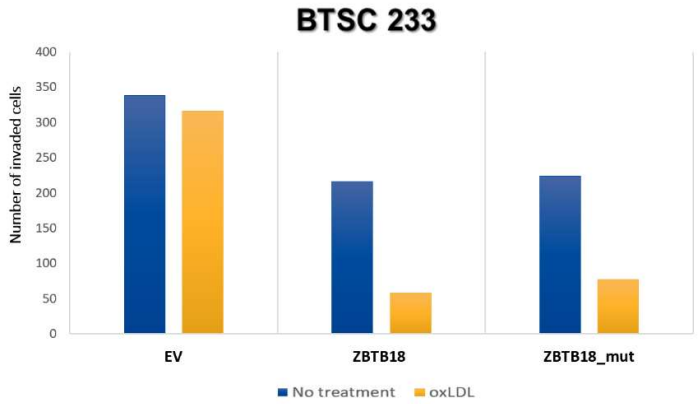

Figure 17: Invasion assay analysis of transduced BTSC 233 treated with oxLDL. The number of invaded cells was decreased in treated cells.

4.3 SREBP gene transcriptional regulation upon ZBTB18 knockdown

We then planned to further analyze the ZBTB18 function by performing CRISPR/Cas9 knockdown in the BTSC475 cells which express a basal level of ZBTB18, by using specific small guide RNAs (sgRNAs) (Provided by Carro's group). Western blot analysis showed that sgRNAs (sgZBTB18#3 and sgZBTB18#4) successfully knocked-down ZBTB18. Upon selection with specific antibiotics, clones were established by limiting dilution. Western blot analysis also demonstrated the successful knockdown of ZBTB18 in those selected single clones "sgZBTB18#3 Cl.53 and sgZBTB18#4 Cl.24" using anti-ZNF238 antibodies and normalizing with α-Tubulin. One of the two bands in sgZBTB18#4 Cl.24 completely disappeared as compared to the EV (Fig.18B,C).

Sequencing results also confirmed that ZBTB18 was successfully edited as demonstrated by the addition of extra nucleotides (Fig. 18A).

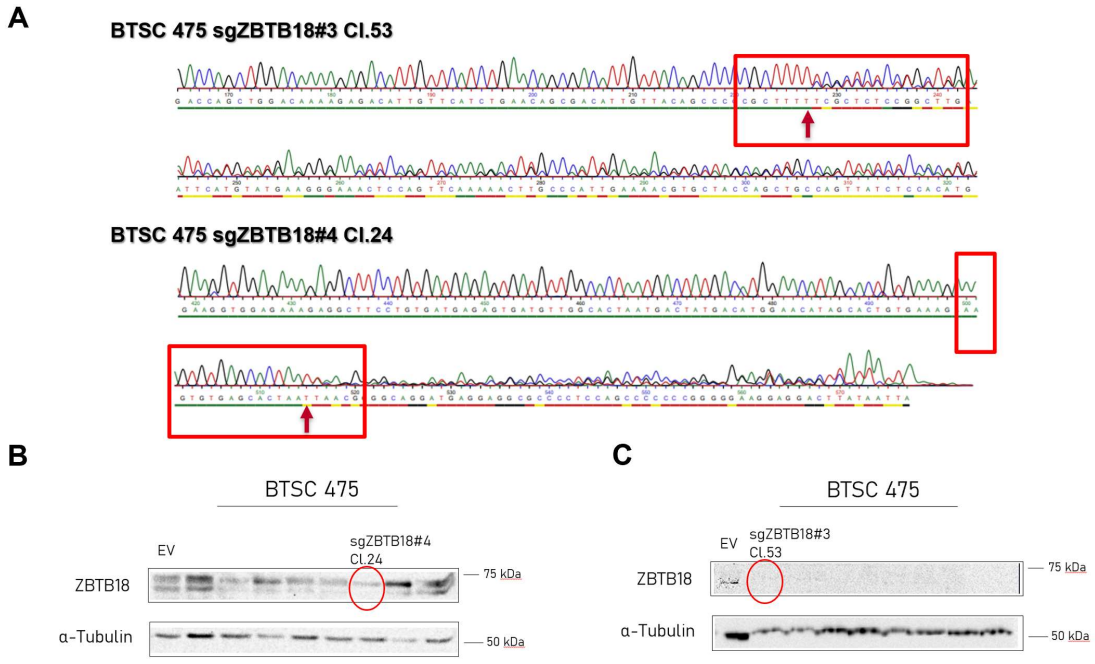

Figure 18: ZBTB18 knock-down using two selected sgRNA. A. Sequencing results of established ZBTB18 knock-down clones in BTSC475. B,C. Western blot analysis of ZBTB18 expression in BTSC475 cells upon ZBTB18 knockdown in clones (sgZBTB18#3 Cl.53 and sgZBTB18#4Cl.24) using anti-ZBTB18 antibodies and normalize with α-Tubulin.

The average analysis of three biological replicates of qPCR revealed that only the expression level of *SCD* and *LDLR* was significantly increased, although it was quite modest and only with sgZBTB18#4 Cl.24. Therefore, as the effect on SREBP genes was very modest in the gene upregulation upon ZBTB18 knockdown, it can be concluded that ZBTB18 level in BTSC475 was very low (Fig 19A,B).

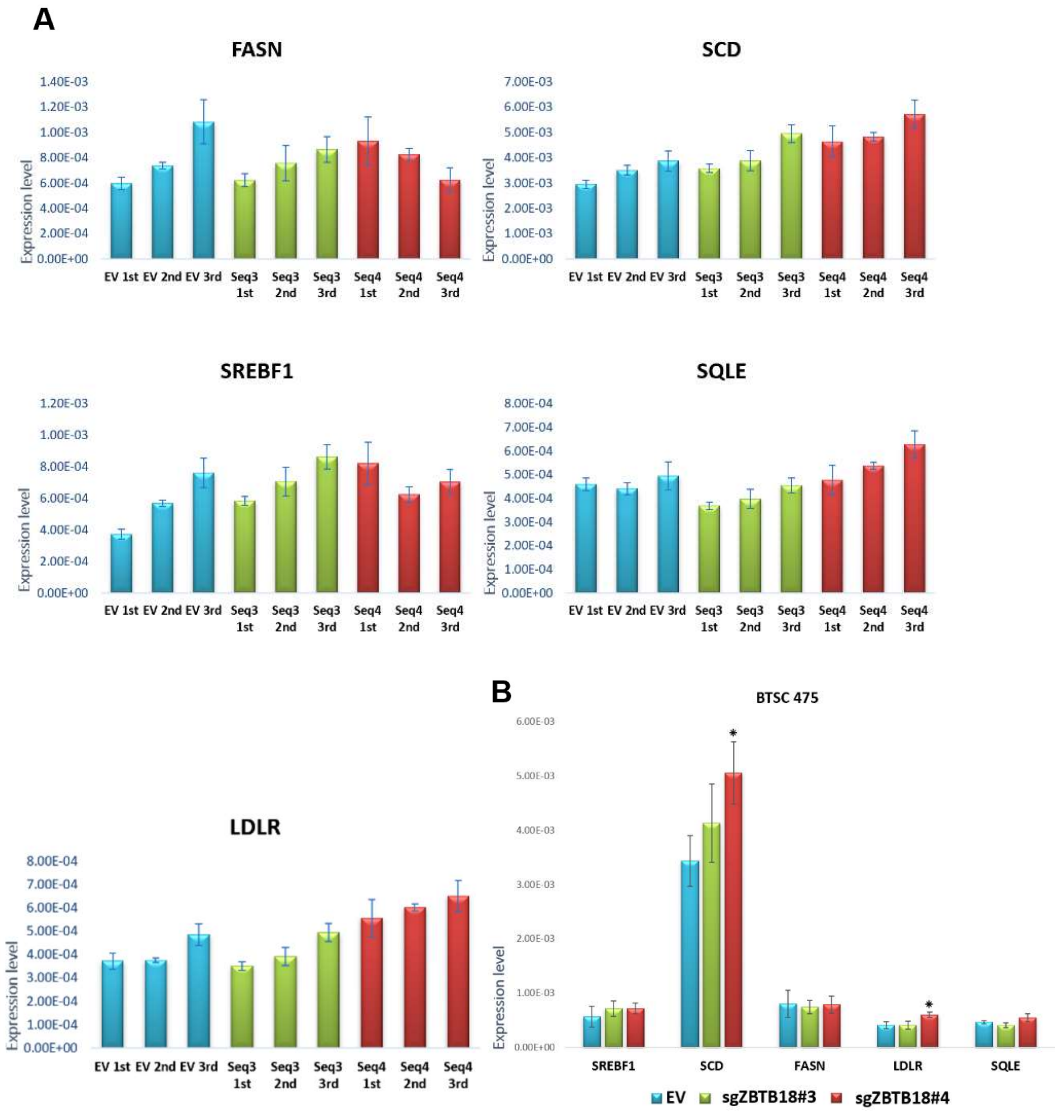

Figure 19: qPCR analysis of selected SREBP targets in BTSC475 cells upon ZBTB18 knockdown. A. The average and standard deviation refer to 3 technical replicates. B. *SCD* and *LDLR* showed a very modest upregulation, and they were only significant with sgZBTB18#4 upon ZBTB18 knockdown. n=3; error bars ± s.d. *p < 0.05, **p <0.01, ***p < 0.001

4.4 Effect of ZBTB18 knockdown on lipid synthesis and cell metabolism

Then, we performed phenotypic assays to investigate whether the absence of ZBTB18 and the consequent expected increase in fatty acid synthesis, affect cell properties which are hallmarks of tumorigenesis. In particular, we analyzed cell lipid droplet content and cell metabolic activity.

Our data showed that the lipid droplet content of ZBTB18 knockdown cells was significantly increased compared to the cells transduced with an empty vector (EV) (Fig. 20A, B).

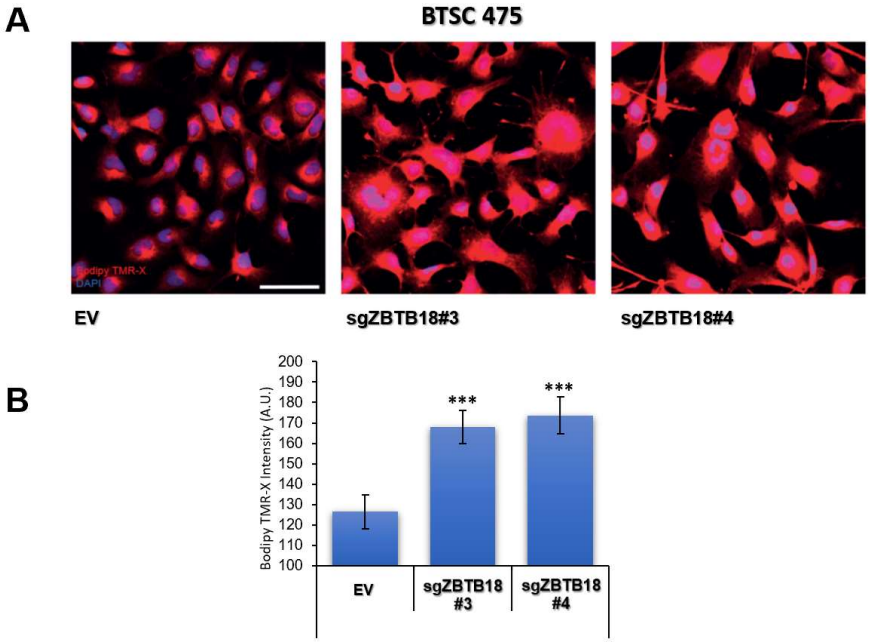

Figure 20: ZBTB18 knockdown increases lipid accumulation in the cells and reduces aerobic respiration. A Bodipy TMR-X lipid staining of BTSC475 cells expressing EV or ZBTB18 knockdown (sgZBTB18#3 & sgZBTB18#4), grown in lipid-containing medium (Normal medium). Nuclei were counterstained with DAPI. Scale bar: 100µm. B. Quantification of the lipid staining shown in (A). n=5; error bars ± s.d. *p < 0.05, **p < 0.01, ***p < 0.001.

Since fatty acids are a source of energy for mitochondrial respiration in the cell, we investigated whether ZBTB18-mediated regulation of lipid biosynthesis also affects cell metabolism. Therefore, we performed an ATP production rate assay in BTSC475 upon ZBTB18 knockdown. To distinguish the ATP production rate in the EV or ZBTB18 knockdown

cells, oxygen consumption rate (OCR) and extracellular acidification rate (ECAR) were measured (Fig.21 A,B). ZBTB18 knockdown expressing cells (sgZBTB18#3 and sgZBTB18#4) showed a lower total ATP production rate compared to control cells; however, the sgZBTB18#4 indicated a mild effect on the glycolysis ATP production rate. The contribution to the reduction in mitochondrial respiration rate in sgZBTB18#4 led to a reduction in overall ATP production rate as compared to the EV. The sgZBTB18#3 cells, howbeit, didn't show a reliable effect even in the glycolysis ATP production rate. This was probably due to suffering observed according to cell appearance changes (Fig. 21C,D).

Largely, our data suggest that ZBTB18 knockdown may authorize the tumor cells to receive their energy from the aerobic respiration with fatty acids, although, the cells might prefer some of the other external sources available.

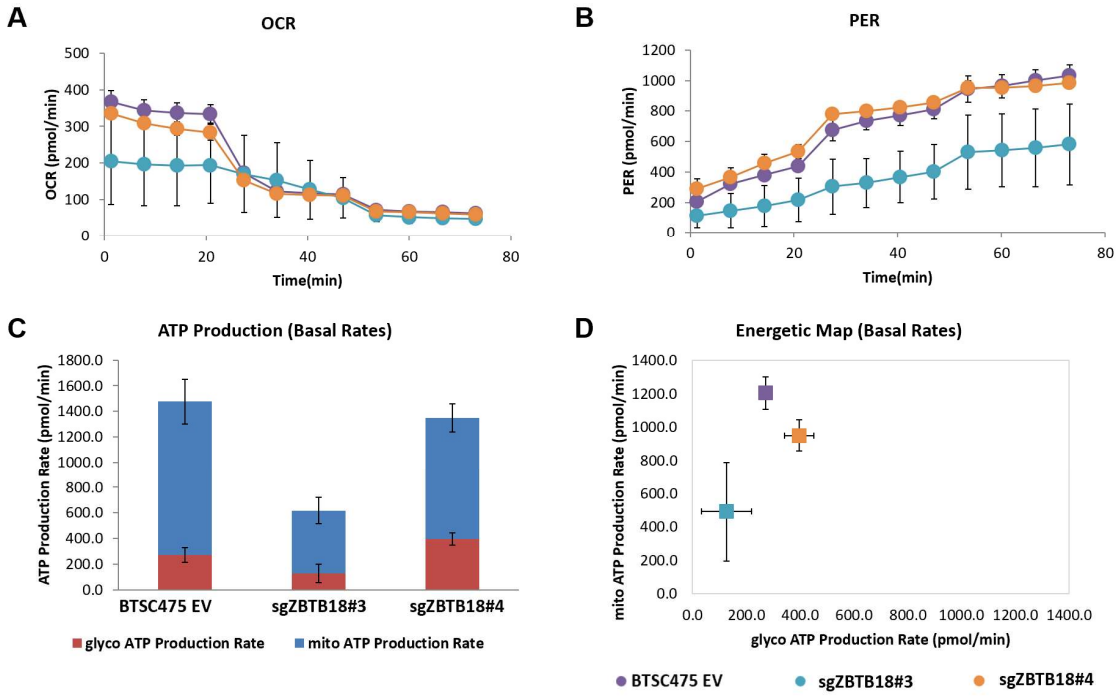

Figure 21: Metabolic activity in BTSC475 cells upon ZBTB18 knockdown. A.Oxygen consumption rate (OCR) measured in a Seahorse ATP production rate assay in either oligomycin or rotenone/antimycin A that were added at given time points for each experiment. B. Extracellular acidification rate (ECAR) measured in a Seahorse ATP production rate assay C. Stacked bar graph showing the glycolytic and mitochondrial contribution to the ATP production rate for each sample D. Graphical representation of the cell energy phenotype of the mentioned samples.

4.5 Effect of HDAC and LSD1 inhibition in SREBP transcriptional regulation

Previous data from the Carro's group have shown that the histone demethylase *LSD1* is implicated in SREBP activation. In addition, more recent data also suggested that the histone deacetylase *HDAC1*/2 may play a similar role. Here, we planned to investigate the effect of inhibition both *LSD1* and *HDAC* using Corin, a recently established and characterized (Anastas et al., 2019). To establish the correct condition to inhibit the effect of *HDAC* deacetylation and *LSD1* demethylation activity, various brain tumor stem-like cells (BTSC168 and BTSC475 cells) were treated with two different concentrations of Corin (0.5 µM and 1.0 µM) and harvested 2 and 6 days after treatment. Monitoring the cells showed that the cells were suffering differently upon Corin treatment (i.e., reduction of cell adhesion and floating of the cells) especially in higher concentration and exposure time (1.0 µM for 6 days).

To test the effect of Corin, western blot analysis on nuclear lysates was performed to examine changes in the level of the epigenetic markers. The time-course experiment with different Corin treatments showed that both markers raised in their abundance, indicating that both *HDAC* deacetylation and *LSD1* demethylation activity were inhibited. Among the conditions tested, 2 days treatment with 1.0 µM Corin produced the best result (Fig.22A).

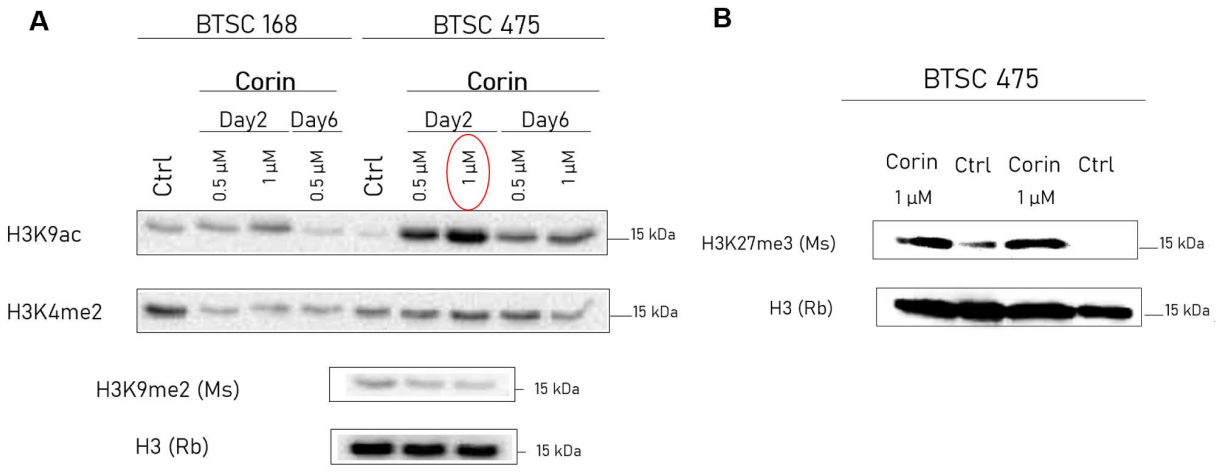

Figure 22: Western blot analysis of LSD1 and HDAC expression in BTSC475 cells upon treatment with Corin inhibitor using antibodies directed against H3K9ac, H3K4me2, and H3K27me3. Anti-Histone 3 (H3) detection was used as a loading control.

In addition, we tested H3K27me3 which has also been reported to be demethylated by *LSD1* (Anastas et al., 2019). We observed a clear increase in H3K27me3 levels, consistent with the previous results, further indicating that *LSD1* demethylation activity has been inhibited (Fig.22B).

Then, we tested whether *LSD1* and *HDAC* inhibition by Corin affected SREBP gene expression, using the conditions established above (1.0 μM Corin for 2 days). Analysis of five independent experiments by qPCR showed a significant reduction of *SQLE* expression and a lesser, but still significant, decrease of *FASN* and *SREBF2* expression. *SCD* mRNA level expression didn't show a significant result although a trend of reduction upon Corin treatment could be observed (Fig.23). These data suggest that *LSD1* and *HDAC* inhibition negatively regulate SREBP gene expression.

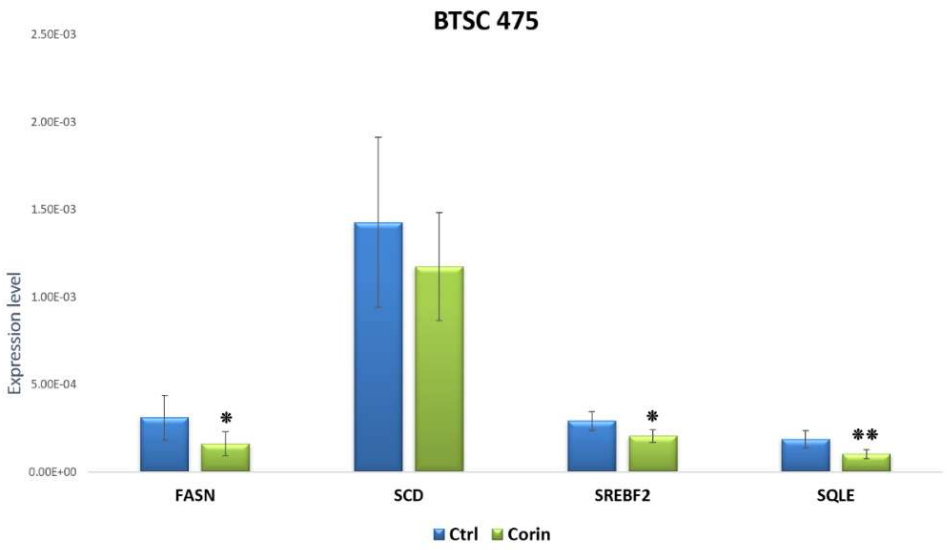

Figure 23: LSD1 and HDAC inhibition negatively regulate SREBP gene expression. qPCR analysis of selected SREBP targets in BTSC475 cells upon Corin treatment. The average and standard deviation refer to 5 technical replicates. The majority of the genes downregulated in treated cells. n=5; error bars ± s.d. *p < 0.05, **p <0.01, ***p < 0.001.

4.6 Effect of HDAC and LSD1 inhibition on lipid synthesis and cell metabolism

Then, we performed lipid droplets (LDs) and metabolism activity to investigate whether the inhibition of *HDAC* and *LSD1* affects the accumulation of lipids and cholesterol, as well as ATP production rate within the cells. Unexpectedly, the amount of lipid droplets did not decrease upon *HDAC* and *LSD1* inhibition as no significant changes were observed between control cells and cells treated with Corin (Fig.24).

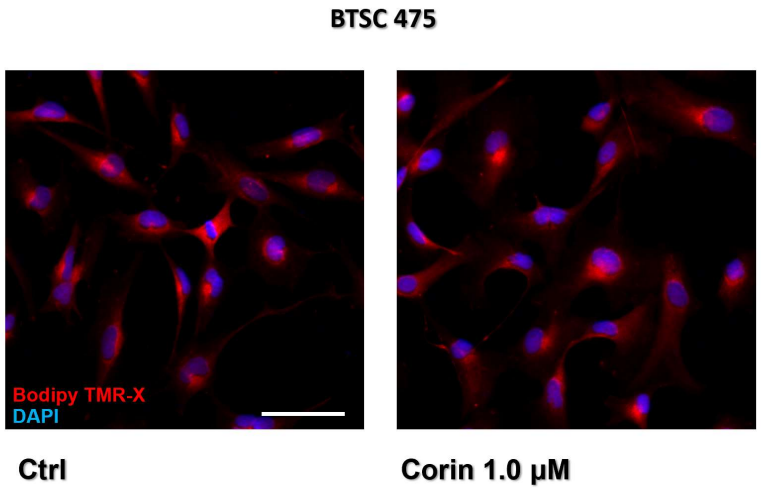

Figure 24: Lipid droplet assay upon Corin treatment of BTSC475. Corin treatment didn't change lipid accumulation in the cells. A Bodipy TMR-X lipid staining was used for BTSC475 cells grown in a lipid-containing medium (Normal medium). Nuclei were counterstained with DAPI. Scale bar: 100µm.

ATP production rate assay showed a slight reduction in the total ATP production when *LSD1* and HDAC were blocked by Corin compared to the ctrl cells. Oxygen consumption rate (OCR) and extracellular acidification rate (ECAR) were measured to survey the ATP production rate in the Ctrl or Corin-treated cells (Fig. 25A,B). Whereas the glycolytic contribution increased in the treated cells compared to the normal conditions, the reduction in mitochondrial respiration led to an overall reduction in ATP production. No significant reduction was observed in the treated cells since the reduction of mitochondrial respiration was not as growing as of the glycolysis between samples treated with Corin and in normal conditions.

In general, our data suggest that the inhibition of *HDAC* and *LSD1* activity may reduce one of the multiple sources of energy for tumor cells although it has no strong effect on fatty acid synthesis (Fig. 25C,D).

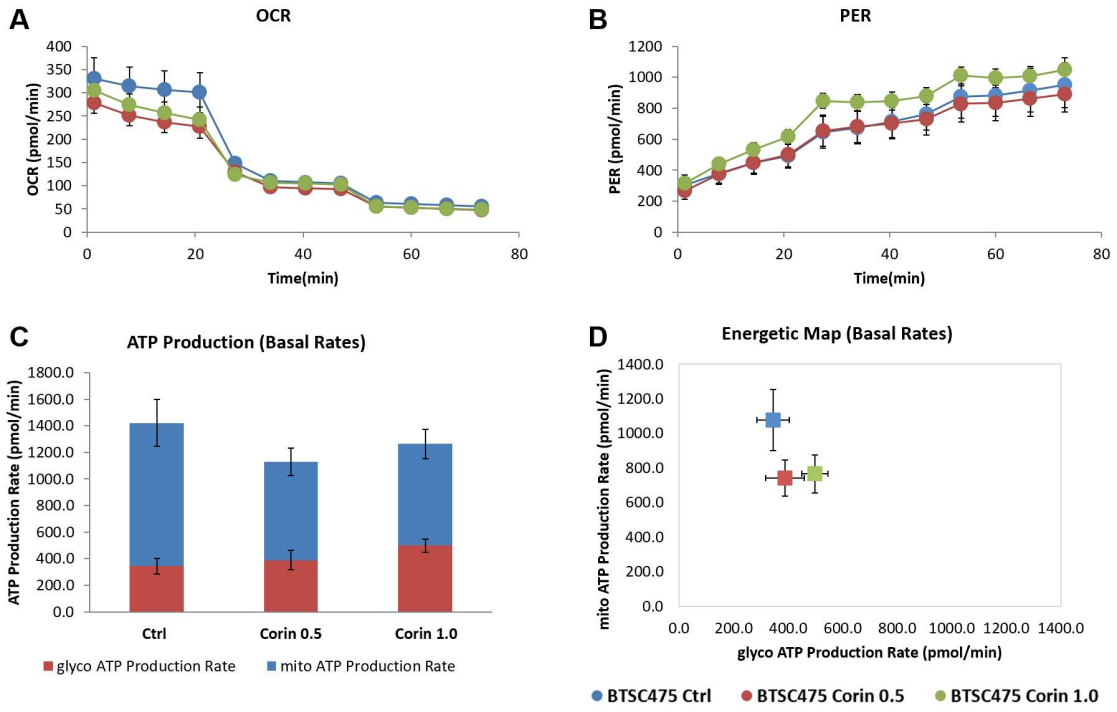

Figure 25: Metabolic activity in BTSC475 cells upon Corin treatment. A. Oxygen consumption rate (OCR) measured in a Seahorse ATP production rate assay in either oligomycin or rotenone/antimycin A that were added at given time points for each experiment. B. Extracellular acidification rate (ECAR) measured in a Seahorse ATP production rate assay C. Stacked bar graph showing the glycolytic and mitochondrial contribution to the ATP production rate for each sample D. Graphical representation of the cell energy phenotype of the mentioned samples.

5 Discussion

A previous study (Carro et al., 2010) provided evidence of the role of ZBTB18 in a network of mesenchymal transformation in glioblastoma. More recently data from Carro's group showed that overexpression of ZBTB18 led to a loss of the mesenchymal and proliferative signatures, and downregulation of an array of genes involved in glioblastoma tumorigenesis (Fedele et al., 2017). These surveys supported the role of ZBTB18 as a tumor suppressor in glioblastoma and raised further questions as to how this is carried out in tumor samples. This thesis described the mechanisms by which ZBTB18 targets lead to glioblastoma progression. Recently, Dr. Carro's group has reported that ZBTB18 regulates the expression of SREBP genes which was involved in fatty acid synthesis. Here, this study could better define the activation of the SREBP pathway and whether this plays a role in the previously observed ZBTB18-mediated phenotype in GBM (Ferrarese R et al., 2020). This study also focused on the epigenetic changes associated with SREBP gene regulation and investigated the potential use of a dual histone deacetylase and histone demethylase inhibitor as a drug to inhibit fatty acid synthesis in glioblastoma (Ferrarese R et al., 2020 and DK Project from the group).

5.1 Role of SREBP genes in ZBTB18-mediated tumor suppressor function

Our time-course experiment with different oxLDL conditions clearly showed that oxLDL treatment in BTSC233 was more effective after 5 days. For BTSC168 none of the first treatments (3, 5, and 7 days) was appropriate and therefore we performed a second test with shorter treatments. Among the selected genes were tested, *GPAM* was the only one that appeared to be upregulated, at day 7. It is important to mention that when cells were treated for 7 days the cell medium had to be replaced at day 5 due to the high number of growing cells in the plate, which could have produced some artifacts (Fig 12A). When BTSC168 cells were treated for 48h with oxLDL a clear upregulation of the genes tested was observed (Fig 12B).

Analysis of SREBP gene expression by qPCR in BTSC168 cells transduced with ZBTB18 or ZBTB18-mut and treated with oxLDL did not work as expected, based on the initial tests, neither for ZBTB18 repression nor for oxLDL induction. Besides, BTSC233 cells also did not show significant changes. The major problem appeared to be the lack of induction of SREBP genes upon oxLDL, differently from the initial setup experiment (Fig.12 and Fig. 14). This might be due to technical reasons that were not figured out. Therefore, this experiment remains unconclusive.

The results from apoptosis in BTSC168 showed that ZBTB18 and ZBTB18_mut induced apoptosis and this is slightly counteracted by oxLDL; however, since the treatment with oxLDL did not appear to be optimal it is not possible to drive a clear conclusion (Fig.15A,B).

In a survey on colon tumor cells, the authors showed that ZBTB18 re-expression significantly reduced proliferation in vitro and a subcutaneous xenograft mouse model (Bazzocco et al, 2021). The proliferation rate in BTSC233 transduced with ZBTB18 and ZBTB18_mut appeared to be reduced as compared to the control, as expected (Fig. 16A,B). In the invasion assay, we observed fewer invading cells in the ZBTB18 and ZBTB18_mut compared to the EV (Fig. 17). This observation confirms that in the presence of ZBTB18, cell proliferation reduces.

Due to the fact that previous studies connected the SREBP pathway to the most aggressive type of GBM (Ferrarese R et al., 2020), we expected that activation of the SREBP pathway as a result of oxLDL, would increase cell invasion and proliferation and perhaps overcome ZBTB18-mediated effect (i.e., reduction of proliferation and invasion). However, due to technical reasons that still need to be clarified, our experiments did not allow us to rule out whether ZBTB18-mediated downregulation of SREBP genes is important for ZBTB18 tumor suppressor activity and therefore should be repeated.

5.2 ZBTB18 knockdown positively regulates SREBP gene expression and lead to increased lipids droplet content

To further prove the role of ZBTB18 as a negative regulator of SREBP genes, we knocked down ZBTB18 in BTSC475 cells, by CRISPR/Cas9. ZBTB18 loss was proved by western blot and confirmed by Sanger sequencing (Fig 18A,B, and C). Initial analysis of SREBP gene analysis by other co-workers in the lab revealed a modest downregulation upon ZBTB18 knocked down. Therefore, we decided to establish single clones by limiting dilution. Gene expression analysis of selected SREBP gene targets by qPCR showed that, upon ZBTB18 knockdown, the majority of SREBP genes were upregulated at the level of gene expression as we expected from the previous studies. qPCR analysis of three biological replicates indicated that the majority of the SREBP genes appeared to be regulated, although the overall change was not dramatic, probably as a consequence of the low ZBTB18 level in the cells (Fig. 19). Following the results of the gene expression analysis, the accumulation of lipid droplets inside the cells also increased (Fig. 20)

Geng and colleagues reported *SOAT1* (sterol-O transferase 1) had a rule in SREBP regulation since it is a main enzyme implicated in the formation of LD in GBM. They also showed that *SOAT1* inhibition blocks cholesterol esterification, resulting to repress GBM growth and enhance survival in xenograft models via block of SREBP-1-regulated lipid synthesis (Geng.Guo 2017; Geng et al., 2016). More recent results indicated ZBTB18 affects lipid biosynthesis, although, it was not able to influence the ability of GBM cells to gather lipids from external sources (Ferrarese R. et al., 2020).

Since a recent study by the group assert that ZBTB18 overexpression controls cell metabolism we planned to investigate whether ZBTB18 knockdown also has an impact on the cell metabolic activity, by performing an ATP production rate assay. To decipher whether ZBTB18 knockdown affects mitochondrial respiration and glycolysis, both Oxygen consumption rate (OCR) and extracellular acidification rate (ECAR) were measured to identify the ATP production rate in the cells transduced with empty vector (EV) or sgZBTB18 (Fig. 21A,B). We

observed a lower ATP production rate in ZBTB18 knockdown expressing cells (sgZBTB18#3 and sgZBTB18#4) compared to normal expressing ZBTB18 cells suggesting that ZBTB18 knockdown may lead the tumor cells to receive their energy from the aerobic respiration with fatty acids, although, the cells might prefer some of the other external sources that are available (Fig. 21C,D).

In general, this study addressed the absence of ZBTB18, upregulated the expression of SREBP targets, and led to an excess of lipids in lipid droplets due to more fatty acid synthesis although no specific effect was observed in the cell metabolic activity.

5.3 *LSD1* and *HDAC* inhibition negatively regulated SREBP gene expression and led to reduction of cell metabolism

Carro's group discovered that *LSD1* and *HDAC* were implicated in SREBP activation. In this thesis, we investigated the effect of inhibiting *HDAC* and *LSC1* using Corin which was capable to act as a dual inhibitor of HDAC-mediated deacetylation and *LSD1*-mediated demethylation activity (Anastas et al., 2019).

Corin has been shown to increase H3K27me3 levels which were suppressed by H3K27M (K27 methionine (M) substitution in H3) mutant histones, and at the same time increases H3K4me1 (LSD1 target) and H3K27ac (HDAC target) at differentiation-associated genes. (Anastas et al., 2019). From a therapeutic point of view, the reversibility of epigenetic modifications is conceded in many tumors due to the biological characteristics of glioblastoma which links to these alterations such as *IDH1/2* mutations (they participate in "epigenetic modifier" enzymes), histone 3 mutations in variants H3.1 and H3.3 (change the global H3K27me3 levels) and the altered expression of histone methyltransferases and demethylases.

A study held that several melanoma cells were affected by the toxicity of Corin as it exhibits a superior anti-proliferative profile which is showed less toxic to melanocytes and keratinocytes. Moreover, Corin slowed tumor growth in a melanoma mouse xenograft model (Kalin et al.,

2018). Other investigators reported that treating DIPG cells with Corin induced cellular differentiation type, altered histone modifications to promote differentiation and blocked cell cycle, induced cell death, and controlled transcriptional changes associated with increased survival in patients. This study claimed a correlation between Corin-dependent histone PTM changes and decreases in the viability of DIPG cells (Anastas et al., 2019).

Monitoring the cells in our experimental procedures showed that Corin treatment slowed the growth of BTSC475 cells. Cells treated with a higher dose of Corin (1 μM) suffered more compared to cells exposed to a lower dose (0.5 μM), for 6 days. However, when cells were treated with 1.0 μM Corin for a shorter time (2 days), a robust change in histone post-translational modifications (PTM) was observed (Fig. 22).

As displayed by western blot analysis, all of the tested epigenetic modifications (H3K9ac, H3K27me3, and H3K4me2) increased in their abundance through the inhibition of *HDAC* deacetylation and *LSD1* demethylation activity. Then, qPCR analysis was performed to investigate the effect of Corin treatment at the level of gene expression. Under the selected condition (2 days treatment with 1 μM Corin), the mRNA level of selected target genes was reduced. *HDAC* and *LSD1* inhibition demonstrated a significant decrease in *SQLE* expression and a significant decline of *FASN* and *SREBF2* expression while *SCD* tended to be downregulated although it did not reach statistical significance (Fig. 23). Overall, these data suggest that *LSD1* and *HDAC* act as positive regulators of SREBP gene expression.

Analysis of lipid droplets (LDs) contents, unexpectedly, didn't follow the trend we observed at the level of gene expression. Comparing the cells in normal conditions and Corin treatment implied no reliable changes in the accumulation of lipids suggesting that some other pathway might be involved in this process (Fig. 24). Measuring ATP production rate by preventing *LSD1* and *HDAC* activity, in contrast, showed a slight reduction in the total ATP production rate compared to control cells. Oxygen consumption rate (OCR) and extracellular acidification rate (ECAR) were measured (Fig.25 A,B). An increase in the glycolytic ATP production was observed in the Corin-treated cells; however, the ATP rate resulting from mitochondrial

respiration diminished, which resulted in the overall reduction in ATP production although not significant.

In conclusion, our findings suggest that *LSD1* and *HDAC* inhibition negatively regulated SREBP genes and have a mild effect on cell metabolism without a specific effect on lipid droplet content within the cells (Fig.25 C,D). This suggests that other regulators of fatty acid synthesis may still be active. Therefore, further studies will be required to better characterize the complete mechanism of SREBP pathway regulation in glioblastoma cells.

6 Conclusion

Some recent studies have provided evidence that ZBTB18 functions as a tumor suppressor in a network of mesenchymal transformation in glioblastoma. ZBTB18 overexpression lead to a loss of the mesenchymal and proliferative signatures and downregulation of an array of genes involved in glioblastoma tumorigenesis. ZBTB18 also regulates the expression of SREBP genes which are involved in fatty acid synthesis.

With the goal to better describe the mechanisms by which ZBTB18 targets lead to glioblastoma progression, we first focused on the activation of the SREBP pathway using oxLDL, which has been shown to induce SREBP. However, due to technical reasons that still need to be clarified, our experiments did not allow us to rule out whether ZBTB18-mediated downregulation of SREBP genes is important for ZBTB18 tumor suppressor activity.

In addition, to further prove the role of ZBTB18 as a negative regulator of SREBP genes, we knocked down ZBTB18 using CRISPR/Cas9. In general, our investigation addressed the absence of ZBTB18, upregulated the expression of SREBP targets, and led to an excess of lipids in lipid droplets due to more fatty acid synthesis although no specific effect was observed in the cell metabolic activity.

Finally, our study focused on the epigenetic changes associated with SREBP gene regulation and investigated the potential use of a dual inhibitor (Corin) to inhibit fatty acid synthesis in glioblastoma. Our findings revealed that *LSD1* and *HDAC* inhibition negatively regulate SREBP genes and have a mild effect on cell metabolism without a specific effect on lipid droplet content, which suggest that other regulators of fatty acid synthesis may still be active. Therefore, further studies will be required to better characterize the complete mechanism of SREBP pathway regulation in glioblastoma cells.

7 References

Agnihotri S, Aldape KD, Zadeh G. (2014). “Isocitrate dehydrogenase status and molecular subclasses of glioma and glioblastoma“. *Neurosurg Focus,* 37(6): E13. doi:10.3171/2014.9.FOCUS14505

Anastas JN, Zee BM, Kalin JH, Kim M, Guo R, Alexandrescu S, Blanco MA, Giera S, Gillespie SM, Das J, Wu M, Nocco S, Bonal DM, Nguyen Q, Suva ML, Bernstein BE, Alani R, Golub TR, Cole PA, Filbin MG, Shi Y. (2019). “Re-programing Chromatin with a Bifunctional LSD1/ HDAC Inhibitor Induces Therapeutic Differentiation in DIPG“. *Cancer Cell,* 36(5): 528-544. doi: 10.1016/j.ccell.2019.09.005

Basso K, Margolin A, Stolovitzky G, Klein U, Dalla-Favera R, Califano A. (2005). “Reverse engineering of regulatory networks in human B cells“. *Nature genetics*, 37(4): 382-390. doi: 10.1038/ng1532

Bazzocco S, Dopeso H, Martínez-Barriocanal, Á, Anguita E, Nieto R, Li J, García-Vidal E, Maggio V, Rodrigues P, Guimarães de Marcondes P, Schwartz Jr S, A. Aaltonen L, Sánchez A, Mariadason JM, Arango D. (2021). “Identification of ZBTB18 as a novel colorectal tumor suppressor gene through genome-wide promoter hypermethylation analysis“. *Clinical Epigenetics*, 13(88): doi: 10.1186/s13148-021-01070-0

Bitorina AV, Oligschlaeger Y, Ding L, Yadati T, Westheim A, Houben T, Vaes RDW, Damink SWO, Theys J, Shiri-Sverdlov R. (2021). “OxLDL as an Inducer of a Metabolic Shift in Cancer Cells“. *Journal of Cancer,* 12(19): 5817-5824. doi:10.7150/jca.56307

Bozza PT, Viola JPB. (2010). “Lipid droplets in inflammation and cancer“. *Prostaglandins Leukot Essent Fatty Acids*, 82(4-6): 243-250. doi: 10.1016/j.plefa.2010.02.005

Bradford M. M. (1976). “A rapid and sensitive method for the quantitation of microgram quantities of protein utilizing the principle of protein-dye binding“. *Analytical Biochemistry*, 72: 248-254.

Bustin SA. (2002). “Quantification of mRNA using real-time reverse transcription PCR (RT-PCR): trends and problems“. *Journal of Molecular Endocrinology*, 29(1): 23-39. doi: 10.1677/jme.0.0290023

Carro MS, Lim WK, Alvarez MJ, Bollo RJ, Zhao X, Snyder EY, Sulman EP, Anne SL, Doetsch F, Colman1 H, Lasorella A, Aldape K, Califano A, Iavarone A. (2009). “The transcriptional network for mesenchymal transformation of brain tumours“. *Nature*, 463: 318-325. doi: 10.1038/nature08712

Chinnadurai G. (2002). “CtBP, an Unconventional Transcriptional Corepressor in Development and Oncogenesis“. *Molecular Cell*, 9(2): 213-224. doi: 10.1016/S1097-2765(02)00443-4

Chow LML, Endersby R, Zhu X, Rankin S, Qu C, Zhang J, Broniscer A, Ellison DW, Baker SJ. (2011). “Cooperativity within and among Pten, p53, and Rb Pathways Induces High-Grade Astrocytoma in Adult Brain“. *Cancer Cell*, 19(3): 305-316. doi: 10.1016/j.ccr.2011.01.039

Crocetti E, Trama A, Stiller C, Caldarella A , Soffietti R, Jaal J, Weberf DC, Ricardi U, Slowinski J, Brandesi A. (2012). “Epidemiology of glial and non-glial brain tumours in Europe“. *European Journal of Cancer*. 48(10): 1532-42. doi:10.1016/j.ejca.2011.12.013

Dcona MM, Morris BL, Ellis KC, Grossman SR. (2017). “CtBP- an emerging oncogene and novel small molecule drug target: Advances in the understanding of its oncogenic action and identification of therapeutic inhibitors“. *Cancer Biology & Therapy*, 18(6): 379-391. doi:10.1080/15384047.2017.1323586

Dorotea D, Koya D, Ha H. (2020). “Recent Insights Into SREBP as a Direct Mediator of Kidney Fibrosis via Lipid-Independent Pathways“. *Frontiers in Pharmacologyl*, 11: 265. doi: 10.3389/fphar.2020.00265

Fedele V, Dai F, Masilamani AP, Heiland DH, Kling E, Gätjens-Sanchez AM, Ferrarese R, Platania L, Soroush D, Kim H, Nelander S, Weyerbrock A, Prinz M, Califano A, Iavarone A, Bredel M, Carro MS. (2017). “Epigenetic Regulation of ZBTB18 Promotes Glioblastoma Progression“. *Molecular Cancer Research,* 15(8): 998-1011. doi:10.1158/1541-7786.MCR-16-0494

Ferno J, Skrede S, Vik-Mo AO, Jassim G, Hellard SL, Steen VM. (2011). “Lipogenic effects of psychotropic drugs: focus on the SREBP system“. *Frontiers in Bioscience,* 16: 49-60. doi:10.2741/3675

Ferrarese R, Izzo A, Andrieux G, Lagies S, Bartmuss JP, Masilamani AP, Wasilenko A, Osti D, Faletti S, Schulzki R, Shuai Y, Kling E, Ribecco V, Heiland DH, Tholen SG, Prinz M, Pelicci G, Kammerer B, Börries M, Carro MS. (2020). “ZBTB18 inhibits SREBP-dependent fatty acid

synthesis by counteracting CTBPs and KDM1A/LSD1 activity in glioblastoma“. *bioRxiv - Cancer Biology*, doi:10.1101/2020.04.17.046268

Ferrarese R, Izzo A, Andrieux G, Lagies S, Masilamani AP, Schulzki R, Shuai Y, Kling E, Ribecco V, Wasilenko A, Heiland DH, Prinz M, Kammerer B, Börries M,Carro MS. (2020). “ZBTB18 interacts with CTBP2 and represses SREBP genes to inhibit fatty acid synthesis in glioblastoma*“. bioRxiv - Cancer Biology*, doi:10.1101/2020.04.17.046268

Garg M, Shanmugam MK, Bhardwaj V, Goel A, Gupta R, Sharma A, Baligar P, Kumar AP, Goh BC, Wang L, Sethi G. (2020). “The pleiotropic role of transcription factor STAT3 in oncogenesis and its targeting through natural products for cancer prevention and therapy“. *Medicinal Research Reviews*, 41(3): 1291-1336. doi: 10.1002/med.21761

Geng F, Cheng X, Wu X, Yoo JY, Cheng C, Guo JY, Mo X, Ru P, Hurwitz B, Kim SH, Otero J, Puduvalli V, Lefai E, Ma J, Nakano I, Horbinski C, Kaur B, Chakravarti A , Guo D. (2016). “Inhibition of SOAT1 suppresses glioblastoma growth via blocking SREBP-1-mediated lipogenesis“. *Clinic Cancer Res*earch, 22(21): 5337-5348. doi: 10.1158/1078-0432.CCR-15-2973

Geng F, Guo D. (2017). “Lipid droplets, potential biomarker and metabolic target in glioblastoma“. *Internal medicine review (Washington, D.C.: Online)*, 3(5): doi: 10.18103/imr.v3i5.443

Glaser K. B. (2007). “HDAC inhibitors: Clinical update and mechanism-based potential“. *Biochemical Pharmacology*, 74(5): 659-671. doi: 10.1016/j.bcp.2007.04.007

Goodenberger ML, Jenkins RB. (2012). “Genetics of adult glioma“. *Cancer Genetics*, 205(12): 613-621. doi: 10.1016/j.cancergen.2012.10.009

He F. (2011). “Laemmli-SDS-PAGE “. *Bio101*, e80: doi: 10.21769/BioProtoc.80

Holland EC. (2000). “Glioblastoma multiforme: The terminator“. *Proceedings of the National Academy of Sciences of the United States of America,* 97(12): 6242–6244. doi: 10.1073/pnas.97.12.6242

Hide T, Takezaki T, Nakamura H, Kuratsu J, Kondo T. (2008). “Brain tumor stem cells as research and treatment targets“. *Brain Tumor Pathol*, 25(2): 67-72. doi: 10.1007/s10014-008-0237-5

Horton JD, Goldstein JL, Brown MS. (2002). “SREBPs: activators of the complete program of cholesterol and fatty acid synthesis in the liver“. *The Journal of Clinical Investigation*, 109(9): 1125-31. doi: 10.1172/JCI15593

Horton JD, Shah NA, Warrington JA, Anderson NN, Park SW, Brown MS, Goldstein JL. (2003). “Combined analysis of oligonucleotide microarray data from transgenic and knockout mice identifies direct SREBP target genes“. *Proceedings of the National Academy of Sciences of the United States of America,* 100(21): 12027–12032. doi:10.1073/pnas.1534923100

Kalin JH, Wu M, Gomez AV, Song Y, Das J, Hayward D, Adejola N, Wu M, Panova I, Chung HJ, Kim E, Roberts HJ, Roberts JM, Prusevich P, Jeliazkov JR, Burman SSR, Fairall L, Milano C, Eroglu A, Proby CM, Dinkova-Kostova AT, Hancock WW, Gray JJ, Bradner JE, Valente S, Mai A, Anders NM, Rudek MA, Hu Y, Ryu B, Schwabe JWR, Mattevi A, Alani RM, Cole PA. (2018). “Targeting the CoREST complex with dual histone deacetylase and demethylase inhibitors“. *Nature Communications,* 9(53). doi:10.1038/s41467-017-02242-4

Kleihues P, Ohgaki H. (2000). “Phenotype vs Genotype in the Evolution of Astrocytic Brain Tumors“. *Toxicologic Pathology*, 28(1): 164-70. doi: 10.1177/019262330002800121

Kleihues P, Soylemezoglu F, Schauble B, Scheithauer BW, Burger PC. (1995). “Histopathology, Classification, and Grading of Gliomas“. *Glia*. 15(3): 211-21. doi:10.1002/glia.440150303

Laemmli U. K. (1970). “Cleavage of Structural Proteins during the Assembly of the Head of Bacteriophage T4“. *Nature*, 227(5259): 680-685.

Liu C, Sage JC, Miller MR, Verhaak RGW, Hippenmeyer S, Vogel H, Foreman O, Bronson RT, Nishiyama A, Luo L, Zong H. (2011). “Mosaic Analysis with Double Markers Reveals Tumor Cell of Origin in Glioma“. *Cell*, 146(2): 209-221. doi: 10.1016/j.cell.2011.06.014

Louis DN, Perry A, Reifenberger G, Deimling AV, Figarella-Branger D, Cavenee WK, Ohgaki H, Wiestler OD, Kleihues P, Ellison DW. (2016). “The 2016 World Health Organization Classification of Tumors of the Central Nervous System: a summary“. *Acta Neuropathol*, 131(6): 803-820. doi: 10.1007/s00401-016-1545-1

Maher EA, Furnari FB, Bachoo RM, Rowitch DH, Louis DN, Cavenee WK, DePinho RA. (2001). “Malignant glioma: genetics and biology of a grave matter*“. Genes & Development,* 15(11): 1311-33. doi: 10.1101/gad.891601

Mao XG, Zhang X, Xue XY, Guo G, Wang P, Zhang W, Fei Z, Zhen HN, You SW, Yang H. (2009). “Brain Tumor Stem–Like Cells Identified by Neural Stem Cell Marker CD15“. *Translational Oncology*, 2(4): 247-257. doi: 10.1593/tlo.09136

Mrowczynski OD , Yang AL, Liao J, Rizk E. (2021). “The Potential of Glioblastoma Patient Symptoms to Diagnose and Predict Survival“. *Cureus*, 13(7): e16675. doi:10.7759/cureus.16675

Mulholland S, Pearson DM, Hamoudi RA, Malley DS, Smith CM, Weaver JMJ, Jones DTW, Kocialkowski S, Bäcklund LM, Collins VP,Ichimura K. (2012). “MGMT CpG island is invariably methylated in adult astrocytic and oligodendroglial tumors with IDH1 or IDH2 mutations“. *International Journal of Cancer*, 131(5):1104-1113. doi: 10.1002/ijc.26499

Narula K, Datta A, Chakraborty N, Chakraborty S. (2013). “Comparative analyses of nuclear proteome: extending its function“. *Frontiers Plant Science*, 4(100). doi: 10.3389/fpls.2013.00100

Okado H. (2021). “Nervous system regulated by POZ domain Krüppel-like zinc finger (POK) family transcription repressor RP58“. *British Journal of Pharmacology*, 178(4): 813–826. doi: 10.1111/bph.15265

Ohgaki H, Dessen P, Jourde B, Horstmann S, Nishikawa T, Patre PD, Burkhard C, Schu¨ler D, Probst-Hensch NM, Maiorka PC, Baeza N, Pisani P, Yonekawa Y, Yasargil MG, Lu¨tolf UM, Kleihues P. (2004). “Genetic Pathways to Glioblastoma: A Population-Based Study“. *Cancer Research,* 64(19): 6892-9. doi:10.1158/0008-5472.CAN-04-1337.

Parsons DW, Jones S, Zhang X, Lin JC, Leary RJ, Angenendt P, Mankoo P, Carter H, Siu I, Gallia GL, Olivi A, McLendon R, Rasheed BA, Keir S, Nikolskaya T, Nikolsky Y, Busam DA, Tekleab H, Diaz Jr LA, Hartigan J, Smith DR, Strausberg RL, Marie SKN, Shinjo SMO, Yan H, Riggins GJ, Bigner DD, Karchin RK, Papadopoulos N, Parmigiani G, Vogelstein B, Velculescu VE, Kinzler KW. (2008). “An integrated genomic analysis of human glioblastoma multiforme“. *Science*, 321(5897): 1807-1812. doi: 10.1126/science.1164382

Phillips HS, Kharbanda S, Chen R, Forrest WF, Soriano RH, Wu TD, Misra A, Nigro JM, Colman H, Soroceanu L, Williams PM, Modrusan Z, Feuerstein BG, Aldape K. (2006). “Molecular subclasses of high-grade glioma predict prognosis, delineate a pattern of disease progression, and resemble stages in neurogenesis“. *Cancer Cell,* 9(3): 157-73. doi:10.1016/j.ccr.2006.02.019

Pinz S, Unser S, Buob D, Fischer P, Jobst B, Rascle A. (2015). “Deacetylase inhibitors repress STAT5-mediated transcription by interfering with bromodomain and extra-terminal (BET) protein function“. *Nucleic Acids Research*, 43(7): 3524–3545. doi: 10.1093/nar/gkv188

Ragni E, Vigano M, Rebulla P, Giordano R, Lazzari L. (2013). “What is beyond a qRT-PCR study on mesenchymal stem cell differentiation properties: how to choose the most reliable housekeeping genes“. *Journal of Cellular and Molecular Medicine*, 17(1): 168-180. doi: 10.1111/j.1582-4934.2012.01660.x

Rascle A, Johnston JA, Amati B. (2003). “Deacetylase Activity Is Required for Recruitment of the Basal Transcription Machinery and Transactivation by STAT5“. *Molecular and Cellular Biology*, 23(12): 4162-4173. doi: 10.1128/MCB.23.12.4162-4173.200

Riemenschneider MJ, Jeuken JWM, Wesseling P, Reifenberger G. (2010). “Molecular diagnostics of gliomas: state of the art“. *Acta Neuropathol*, 120(5): 567-584. doi: 10.1007/s00401-010-0736-4

Schmitt MJ, Company C, Dramaretska Y, Barozzi I, Göhrig A, Kertalli S, Großmann M, Naumann H, Sanchez-Bailon MP, Hulsman D, Glass R, Squatrito M, Serresi M, Gargiulo G. (2021). “Phenotypic Mapping of Pathologic Cross-Talk between Glioblastoma and Innate Immune Cells by Synthetic Genetic Tracing“. *Cancer Discovery,* 11(3): 754-778. doi:10.1158/2159-8290.CD-20-0219

Singh MM, Manton CA, Bhat KP, Tsai WW, Aldape K, Barton MC, Chandra J. (2011). “Inhibition of LSD1 sensitizes glioblastoma cells to histone deacetylase inhibitors“. Neuro-Oncology, 13(8): 894–903. doi: 10.1093/neuonc/nor049

Singh MM, Johnson B, Venkatarayan A, Flores ER, Zhang J, Su X, Barton M, Lang F, Chandra J. (2015). “Preclinical activity of combined HDAC and KDM1A inhibition in glioblastoma“. Neuro-Oncology, 17(11): 1463–1473. doi: 10.1093/neuonc/nov041

Song T, Wang P, Li C, Jia L, Liang Q, Cao Y, Dong P, Shi H, Jiang M. (2021). “Salidroside simultaneously reduces de novo lipogenesis and cholesterol biosynthesis to attenuate atherosclerosis in mice“. *Biomedicine & Pharmacotherapy*, 134(111137). doi:10.1016/j.biopha.2020.111137

Tabatabai G, Stupp R, van den Bent MJ, Hegi ME, Tonn JC, Wick W, Weller M. (2010). “Molecular diagnostics of gliomas: the clinical perspective“. *Acta Neuropathol*, 120(5): 585-92. doi: 10.1007/s00401-010-0750-6

Tamimi AF, Juweid M. (2017). “Epidemiology and Outcome of Glioblastoma“. In book*: Glioblastoma*: 143-153. doi: 10.15586/codon.glioblastoma.2017.ch8

Tatard VM , Xiang C , Biegel JA , Dahmane N. (2010). “ZNF238 Is Expressed in Postmitotic Brain Cells and Inhibits Brain Tumor Growth“. *Cancer Research* 70(3): 1236–46. doi: 10.1158/0008-5472.CAN-09-2249

Urbańska K, Sokołowska J, Szmidt M, Sysa P. (2014). “Glioblastoma multiforme – an overview“. *contemporary oncology*, 18(5): 307-312. doi: 10.5114/wo.2014.40559

Vandesompele J, Preter KD, Pattyn F, Poppe B, Roy NV, Paepe AD, Speleman F. (2002). “Accurate normalization of real-time quantitative RT-PCR data by geometric averaging of multiple internal control genes“. *Genome Biology*, 3(7): research0034.1. http://genomebiology.com/2002/3/7/research/0034

Verhaak RGW, Hoadley KA, Purdom E, Wang V, Qi Y, Wilkerson MD, … Hayes DN. (2010). “Integrated genomic analysis identifies clinically relevant subtypes of glioblastoma characterized by abnormalities in PDGFRA, IDH1, EGFR, and NF1”. *Cancer Cell*, *17*(1): 98–110. doi:10.1016/j.ccr.2009.12.020

Walther TC, Farese Jr RV. (2012). “Lipid Droplets and Cellular Lipid Metabolism“. *Annu Rev Biochem*, 81: 687-714. doi: 10.1146/annurev-biochem-061009-102430

Wu W, Klockow JL, Zhang M, Lafortune F, Chang E, Jin L, Wu Y, Daldrup-Link HE. (2021). “Glioblastoma multiforme (GBM): An overview of current therapies and mechanisms of resistance“. *Pharmacological Research*. 171(105780). doi:10.1016/j.phrs.2021.105780.

Xiang C, Frietze KK, Bi Y, Li Y, Pozzo VD, Pal S, Alexander N, Baubet V, D’Acunto V, Mason CE, Davuluri RV, Dahmanea N. (2021). “RP58 Represses Transcriptional Programs Linked to Nonneuronal Cell Identity and Glioblastoma Subtypes in Developing Neurons“. *Molecular and Cellular Biology*, 41(7): e0052620. doi: 10.1128/MCB.00526-20

Zhu Y, Guignard F, Zhao D, Liu L, Burns DK, Mason RP, Messing A, Parada LF. (2005). “Early inactivation of p53 tumor suppressor gene cooperating with NF1 loss induces malignant astrocytoma“. *Cancer Cell*, 8(2): 119-130. doi: 10.1016/j.ccr.2005.07.004